

ARTICLE LINK: <http://www.sciencedirect.com/science/article/pii/S0191261514000022>

PLEASE CITE THIS ARTICLE AS

Han, K., Gayah, V.V., Piccoli, B., Friesz, T.L., Yao, T., 2015. On the continuum approximation of the on-and-off signal control on dynamic traffic networks.

Transportation Research Part B 61, 73-97.

On the continuum approximation of the on-and-off signal control on dynamic traffic networks

Ke Han^{a,*}, Vikash V. Gayah^b, Benedetto Piccoli^c, Terry L. Friesz^d, Tao Yao^d

^aDepartment of Civil and Environmental Engineering, Imperial College London, United Kingdom.

^bDepartment of Civil and Environmental Engineering, Pennsylvania State University, USA.

^cDepartment of Mathematical Sciences and CCIB, Rutgers University - Camden, USA

^dDepartment of Industrial and Manufacturing Engineering, Pennsylvania State University, USA.

Abstract

In the modeling of traffic networks, a signalized junction is typically treated using a binary variable to model the on-and-off nature of signal operation. While accurate, the use of binary variables can cause problems when studying large networks with many intersections. Instead, the signal control can be approximated through a continuum approach where the on-and-off control variable is replaced by a priority parameter. Advantages of such approximation include elimination of the need for binary variables, lower time resolution requirements, and more flexibility and robustness in a decision environment. It also resolves the issue of discontinuous travel time functions arising from the context of dynamic traffic assignment.

Despite these advantages in application, it is not clear from a theoretical point of view how accurate is such continuum approach; i.e., to what extent is this a valid approximation for the on-and-off case. The goal of this paper is to answer these basic research questions and provide further guidance for the application of such continuum signal model. In particular, by employing the *Lighthill-Whitham-Richards* model (Lighthill and Whitham, 1955; Richards, 1956) on a traffic network, we investigate the convergence of the on-and-off signal model to the continuum model in regimes of diminishing signal cycles. We also provide numerical analyses on the continuum approximation error when the signal cycles are not infinitesimal. As we explain, such convergence results and error estimates depend on the type of fundamental diagram assumed and whether or not vehicle spillback occurs in a network. Finally, a traffic signal optimization problem is presented and solved which illustrates the unique advantages of applying the continuum signal model instead of the on-and-off one.

Keywords: traffic signal, continuum approximation, LWR model, convergence, approximation error, vehicle spillback

1. Introduction

Signalized intersections play a vital role in the design, management and control of urban traffic networks. These locations are often the most restrictive bottlenecks, and therefore urban traffic control strategies tend to focus on the operation of signalized intersections (Miller, 1963; Robertson and Bretherton, 1974; Shelby, 2004; Chitour and Piccoli, 2005; Guler and Cassidy, 2012; Gayah and Daganzo, 2012). Thus, it is imperative that we are able to accurately predict traffic dynamics at these locations, and the resulting impact on a network. Fortunately, modeling these common junctions is relatively straightforward: for a given movement at an intersection, the impact of the signal on traffic dynamics is incorporated using a single binary variable. When the signal is green for the subject movement, the binary variable allocates the entirety of the downstream link's capacity to the downstream end of the subject approach. When the signal is red, the binary variable ensures that this capacity is zero.

Unfortunately, the discrete nature of this 'on-and-off' signal timing makes studying and optimizing the control parameters of these junctions rather complex, especially on large networks with many signalized intersections. Incorporating the binary traffic signal state variables in a signal optimization process usually results in mixed integer mathematical programs; examples include Improta and Cantarella (1984), Lo (1999a) and Lo (1999b). For large networks, these mixed integer mathematical programs can be very difficult to solve exactly. Even when possible, the solutions require a tremendous amount of time, which makes real-time applications impossible. Realistic extensions that account for the combination of *dynamic traffic assignment* (DTA) with signal optimization, such as the so-called *dynamic user equilibrium with signal control* (DUESC) problems, become especially difficult (Aziz and Ukkusuri, 2012; Ukkusuri et al, 2013).

To simplify the modeling of signalized intersections in networks, recent studies have proposed an elegant continuum model to approximate traffic dynamics at traffic signals in an intuitive way (Smith, 2010; Ge and Zhou, 2012). This model works as follows. Consider a simple merge junction with two incoming links, I_1 and I_2 , and one outgoing link, I_3 , as depicted in Figure 1. Assume now that the junction A is controlled by a fixed-cycle traffic signal which controls the movement of the exit flows on links I_1 and I_2 . The receiving capacity of the outgoing link I_3 is assumed to be time-dependent and given by the supply function $S_3(t)$. Additionally, the fraction of the cycle dedicated to link I_1 is given by η , and the fraction dedicated to link I_2 is $1 - \eta$ for some $\eta \in (0, 1)$. The continuum model asserts that the proportions η and $1 - \eta$ of the downstream link capacity $S_3(t)$ are assigned to links I_1 and I_2 , respectively, during the entirety of the signal cycle. A more detailed and formal definition of such model will be provided later in Section 2.

While this continuum model will not predict traffic dynamics at the intersection exactly, it does have a number of advantages when compared to the on-and-off signal model that is typically used:

- In a discrete-time setting, the binary representation of signal control strategies will be replaced with a real-valued parameter η . This eliminates the need of using binary variables

*Corresponding author

Email addresses: k.han@imperial.ac.uk (Ke Han), gayah@engr.psu.edu (Vikash V. Gayah), piccoli@camden.rutgers.edu (Benedetto Piccoli), tfriesz@psu.edu (Terry L. Friesz), tyy1@engr.psu.edu (Tao Yao)

for the signalization, and significantly reduces the computational burden of the mixed integer programs such as those reviewed above.

- The on-and-off signal model usually demands a very fine time resolution to accommodate certain signal splits. For example, a cycle with 35 seconds of green phase and 25 seconds of red phase requires a time step of at most 5 seconds to be properly implemented. These fine time resolutions increase the computational requirements of the network simulations and/or optimizations. On the other hand such constraints do not apply to the continuum case, thus one has more flexibility in choosing the time step for computational convenience and efficiency.
- For any fixed-cycle traffic signal optimization problem defined on a prescribed time grid, the on-and-off signal strategy can only take on several discrete values, while the continuum model yields a continuous spectrum of choices and outcomes.
- The on-and-off signal control naturally results in discontinuities in travel time functions, which poses difficulties in quite a few dynamic traffic assignment models. For example, a dynamic user equilibrium problem (Friesz et al., 2013) cannot be properly defined with the on-and-off signal controls unless some sort of indifference of drivers in travel time is introduced (Szeto and Lo, 2006; Ge and Zhou, 2012; Han, 2013). Such obstacle can be easily avoided by the continuum signal model.

Despite the appealing features of the continuum signal model mentioned above, the model has never been rigorously analyzed in connection with its counterpart, the on-and-off model. From an application point of view, it is of fundamental importance to identify circumstances where such continuum approximation accurately describes the aggregate behavior that exists at signalized intersections and, perhaps more importantly, to identify when it is invalid and may induce significant error. It is also worthwhile to investigate to what extent the continuum model is a good approximation of the on-and-off signal control. Solving these objectives can help to identify situations where this approximation can be used, and when its advantages can be realized without sacrificing model accuracy. This serves as the motivation of the current paper and are fully addressed by the findings made herein.

Our analysis of the continuum signal model is based on the network extension of the Lighthill-Whitham-Richards conservation law model that explicitly captures the temporal and spatial distributions of congestion as well as vehicle spillback. This paper employs the most general assumptions on the fundamental diagram to ensure the validity of the convergence result and the error estimates. Our specific findings and/or contributions regarding the continuum signal model are summarized as follows.

- 1(a). For a signalized network, if no spillback¹ occurs on any junction, then the traffic evolution on the network using the on-and-off signal model converges to the solution using a corresponding continuum signal model as the signal cycles tend to zero. This is true for any type of fundamental diagram assumed.
- 1(b). In application, when the signal cycles are not infinitesimal, the difference between the aforementioned two solutions are uniformly bounded if spillback does not occur anywhere

¹In this paper, spillback refers to the situation where the entrance of a link is in the congested phase, causing its supply to drop and affecting the outcome of the junction as well as its immediately preceding links.

in the network. This is again true for any type of fundamental diagram assumed. In addition, expression of such uniform bound is provided explicitly.

- 2(a). If spillback occurs at some junction and lasts for a significant period (e.g., on the scale of several signal cycles), then the above convergence does not hold if the fundamental diagram is triangular, while the convergence continues to hold if the fundamental diagram has a strictly concave congested branch.
- 2(b). Under the same assumption of 2(a), and that the signal cycles are not infinitesimal, the difference between the two solutions grows with time, regardless of the fundamental diagram assumed. However, when using a fundamental diagram with a strictly concave congested branch, the difference is significantly smaller than when a triangular fundamental diagram is assumed. Again, the differences are provided explicitly for any type of fundamental diagram.
3. If spillback takes place and recurs on a smaller time scale (e.g., smaller than a signal cycle), which we call *transient spillback*, then the convergence of the solution with the on-and-off signal model to the one with the continuum signal model does not hold, when the signal cycles tend to zero. Moreover, the approximation error may be very large and grows with time when the signal cycles are not infinitesimal. These statements are true for any fundamental diagram.
4. We provide a traffic signal optimization procedure in the form of a mixed integer linear program which employs either the continuum traffic signal model or the on-and-off signal model. Performances and results of these two programs are compared which highlights the unique advantages of the continuum model and illustrates some of its solution characteristics in line with our theoretical results.

The link dynamics employed in this paper are described by the following first order scalar conservation law:

$$\partial_t \rho(t, x) + \partial_x f(\rho(t, x)) = 0 \quad (t, x) \in [0, T] \times [a, b] \quad (1.1)$$

where $[0, T]$ is some fixed time horizon and the link is expressed as a spatial interval $[a, b]$, $\rho(t, x) \in [0, \rho_j]$ denotes local vehicle density, where ρ_j denotes the jam density. Regarding the fundamental diagram $f(\cdot) : [0, \rho_j] \rightarrow [0, C]$ where C denotes the flow capacity, we impose the following very mild assumptions.

(F) The fundamental diagram $f(\rho)$ is continuous and concave, and vanishes at $\rho = 0$ and $\rho = \rho_j$.

Note that more restrictive constraints are sometimes used throughout this paper when considering the impacts of the continuum approximation when different functional forms of the fundamental diagram are considered.

Analysis of the conservation law models involves shocks and rarefaction waves, which are very case-sensitive especially in the presence of a family of signal controls. Therefore, attacking the proposed problem directly using conservation laws is quite difficult. As part of our contribution in methodology, we invoke the analytical framework of variational theory (Claudel and Bayen, 2010a; Daganzo, 2005; Newell, 1993) and weak value conditions (Aubin et al., 2008) to analyze the models of interest. As we shall demonstrate, solution representation of the signalized

network, asymptotic behavior of the solutions in regimes of diminishing signal cycles, as well as error estimates for the two types of signal models, are all tremendously simplified by considering the variational theory and the weak value conditions.

The rest of this paper is organized as follows. Section 2 introduces additional concepts and notations pertaining to signalized junctions, where the on-and-off and the continuum signal models are formally defined. Section 3 reviews some essential background on variational theory and weak conditions. Section 4 establishes, in the absence of vehicle spillback, convergence of the on-and-off model to the continuum model as the signal cycles tend to zero. We also provide error estimates for the continuum approximation of the on-and-off model when the signal cycles are not infinitesimal. These results are independent of the type of fundamental diagram employed. In Section 5, we conduct similar investigations of convergence and error estimates, assuming that spillback occurs and is sustained at a signalized intersection. The corresponding results are dependent on the type of fundamental diagram employed. Section 6 provides a discussion of convergence in the presence of transient and recurring spillback. Section 7 supports the theoretical results from previous sections using numerical examples. In Section 8, we propose an application of the continuum signal model, namely, a mixed integer linear programming approach for optimal signal timing problem. This is used to illustrate the modeling and computational advantages of the continuum signal model over the on-and-off one, as well as its solution characteristics and qualities. Finally, Section 9 provides some concluding remarks.

2. Signalized junction with fixed cycle and split

In order to illustrate the key features of signalized junctions, we focus on a signalized merge node A , depicted in Figure 1. At this node, there are two incoming links, I_1 and I_2 , and one outgoing link, I_3 . We also note that an additional signal exists at the downstream node B of link I_3 , which will be used to discuss some queue spillbacks in Sections 5 and 7. Although all subsequent results are stated for such junction, extensions of our methodology and insights to more general junctions are straightforward, see more explanation in Section 9.

In signal timing, a period containing one complete green phase and one complete red phase is called a cycle. The cycle length for I_1 (and also for I_2) is denoted by $\Delta_A \in \mathbb{R}_+$. Fix a split parameter $\eta_1 \in (0, 1)$. We let the green time for I_1 be $\eta_1 \Delta_A$ and the green time for I_2 be $(1 - \eta_1) \Delta_A$ in a full cycle.

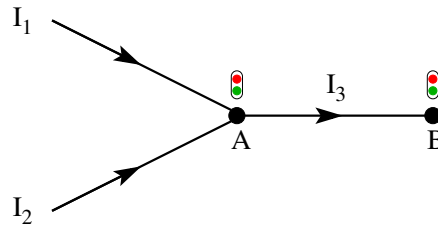


Figure 1: A signalized merge junction.

Each link I_i is expressed as a spatial interval $[a_i, b_i]$, $i = 1, 2, 3$. The density on each link is $\rho_i(t, x)$, $(t, x) \in [0, T] \times [a_i, b_i]$, $i = 1, 2, 3$. We define the demand functions $D_i(t)$ for I_i , $i = 1, 2$

and the supply function $S_3(t)$ for I_3 (Lebacque and Khoshyaran, 1999) as

$$D_i(t) = \begin{cases} C_i & \text{if } x = b_i - \text{ is in the congested phase} \\ f_i(\rho_i(t, b_i-)) & \text{if } x = b_i - \text{ is in the uncongested phase} \end{cases} \quad i = 1, 2 \quad (2.2)$$

$$S_3(t) = \begin{cases} C_3 & \text{if } x = a_3 + \text{ is in the uncongested phase} \\ f_3(\rho_3(t, a_3+)) & \text{if } x = a_3 + \text{ is in the congested phase} \end{cases} \quad (2.3)$$

where $f_i(\cdot)$ is the fundamental diagram, C_i denotes the flow capacity, $i = 1, 2, 3$. Based on $S_3(t)$, we define the *effective supplies* $\mathcal{S}_3^1(t)$ and $\mathcal{S}_3^2(t)$ associated with link I_1 and I_2 respectively as

$$\mathcal{S}_3^1(t) \doteq \min \{C_1, S_3(t)\}, \quad \mathcal{S}_3^2(t) \doteq \min \{C_2, S_3(t)\} \quad (2.4)$$

Quantities $\mathcal{S}_3^1(t)$ and $\mathcal{S}_3^2(t)$ represent, respectively, the capacity provided by the downstream link that is available for I_1 and I_2 to utilize. They will be used to define the on-and-off and the continuum signal models as below.

We consider the periodic, piecewise constant control functions $u_1(t)$ and $u_2(t) : [0, T] \rightarrow \{0, 1\}$, such that

$$u_1(t) = \begin{cases} 1 & \text{when the signal is green for } I_1 \\ 0 & \text{when the signal is red for } I_1 \end{cases} \quad (2.5)$$

$$u_2(t) = \begin{cases} 1 & \text{when the signal is green for } I_2 \\ 0 & \text{when the signal is red for } I_2 \end{cases} \quad (2.6)$$

One obvious identity that must be satisfied by these controls is $u_1(t) + u_2(t) \equiv 1, \forall t \in [0, T]$. One can now write the boundary flows corresponding to an on-and-off control as

$$\left. \begin{aligned} f_1(\rho_1(t, b_1)) &= \min \{D_1(t), \mathcal{S}_3^1(t) \cdot u_1(t)\} \\ f_2(\rho_2(t, b_2)) &= \min \{D_2(t), \mathcal{S}_3^2(t) \cdot u_2(t)\} \\ f_3(\rho_3(t, a_3)) &= f_1(\rho_1(t, b_1)) + f_2(\rho_2(t, b_2)) \end{aligned} \right\} \text{On-and-Off Signal Model} \quad (2.7)$$

where $f_1(\rho_1(t, b_1))$, $f_2(\rho_2(t, b_2))$ denote the exit flows of I_1 and I_2 ; $f_3(\rho_3(t, a_3))$ denotes the inflow of I_3 . On the other hand, the continuum signal model states that

$$\left. \begin{aligned} f_1(\rho_1(t, b_1)) &= \min \{D_1(t), \eta_1 \mathcal{S}_3^1(t)\} \\ f_2(\rho_2(t, b_2)) &= \min \{D_2(t), (1 - \eta_1) \mathcal{S}_3^2(t)\} \\ f_3(\rho_3(t, a_3)) &= f_1(\rho_1(t, b_1)) + f_2(\rho_2(t, b_2)) \end{aligned} \right\} \text{Continuum Signal Model} \quad (2.8)$$

Remark 2.1. *It should be noted that we assume here, as in nearly all first-order traffic flow models, that vehicles accelerate and decelerate instantaneously. Of course, acceleration rates are bounded in reality, and this complication will introduce an additional source of error. In practice, this is usually accounted for by including lost times at the signal where flow is zero, and modeling saturation flows during the effective green time. The methodological framework presented in this paper can be easily modified to incorporate the inclusion of lost times and/or yellow times: simply relax the assumption that the sum of the priority parameters is equal to one and instead let this sum be equal to the fraction of the cycle during which vehicles are allowed to discharge at saturation. This fraction can usually be detrained fairly easily in practice for a given cycle length.*

Although subsequent analyses regarding convergence and error estimate are only stated for link I_1 , the treatment of I_2 is completely symmetric and quite similar.

3. The Hamilton-Jacobi equation and the weak boundary conditions

We introduce the Moskowitz function $N(t, x)$ (Moskowitz, 1965), also known as the Newell-curve (Newell, 1993), which measures the cumulative number of vehicles that have passed location x by time t . The function $N(t, x)$ satisfies the following Hamilton-Jacobi equation

$$\partial_t N(t, x) - f(-\partial_x N(t, x)) = 0 \quad (t, x) \in [0, T] \times [a, b] \quad (3.9)$$

subject to initial condition, upstream and downstream boundary conditions, to be defined below.

3.1. The generalized Lax-Hopf formula

Our analysis of the signalized junction involves a semi-analytical solution representation of the Hamilton-Jacobi equation (3.9) known as the *generalized Lax-Hopf formula* (Aubin et al., 2008; Claudel and Bayen, 2010a,b). For the convenience of invoking weak conditions, we employ a class of lower-semicontinuous viability episolutions of (3.9) in the sense of Barron-Jensen/Frankowska (Barron and Jensen, 1990; Frankowska, 1993).

Let us fix a temporal-spatial domain $[0, T] \times [a, b]$ where $[0, T]$ is the time horizon, $b - a = L$ is the length of the link. The articulation of the generalized Lax-Hopf formula requires the following definition of value conditions.

Definition 3.1. A value condition $C(\cdot, \cdot)$ is a lower-semicontinuous function that maps Ω , a subset of $[0, T] \times [a, b]$, to \mathbb{R} .

Theorem 3.2. (Generalized Lax-Hopf formula) The viability episolution to (3.9) associated with value condition $C(\cdot, \cdot)$ is given by

$$N_C(t, x) = \inf_{(u, \tau) \in \text{Dom}(f^*) \times \mathbb{R}_+} \{C(t - \tau, x - \tau u) + \tau f^*(u)\} \quad (3.10)$$

where $f^*(\cdot)$ is the concave transformation of the Hamiltonian $f(\cdot)$:

$$f^*(u) = \sup_{\rho \in [0, \rho_j]} \{f(\rho) - u\rho\}$$

and $\text{Dom}(f^*) \doteq [f'(0+), f'(\rho_j-)]$.

Proof. The reader is referred to Aubin et al. (2008) for a proof. □

3.2. The weak value conditions

Let us introduce, for equation (3.9), the initial condition $N_{ini}(x)$, the upstream boundary condition $N_{up}(t)$, and the downstream boundary condition $N_{down}(t)$. We make note of the fact that a viability episolution $N(t, x)$ given by (3.10) needs only satisfy the above conditions in an inequality (\leq) sense. In other words, we have

$$N(0, x) \leq N_{ini}(x) \quad \forall x \in [a, b] \quad (3.11)$$

$$N(t, a) \leq N_{up}(t), \quad N(t, b) \leq N_{down}(t) \quad \forall t \in [0, T] \quad (3.12)$$

The reader is referred to Aubin et al. (2008) and Claudel and Bayen (2010a) for more detailed explanation.

Remark 3.3. Throughout this paper, $N_{up}(t)$ is taken as the time-integral of the demand function of the preceding link, rather than the time-integral of the link entry flow; similarly, $N_{down}(t)$ is taken as the time-integral of the supply function of the following link, rather than the time-integral of the link exit flow. Since the demand (supply) of preceding (following) link is usually larger than the actual inflow (outflow) of the link of interest, the boundary conditions $N_{up}(t)$ and $N_{down}(t)$ are satisfied only in an inequality (\leq) sense; in other words, they are weak boundary conditions (Aubin et al., 2008). The advantage of invoking those weak boundary conditions is that solution representation (Lax-Hopf formula) on the link of interest can be obtained without knowledge of the actual inflow or outflow. Moreover, in order to draw any conclusion about the solution, it suffices to investigate $N_{up}(t)$ and $N_{down}(t)$. These two facts greatly simplify our analyses that will follow in Section 4 and 5.

In the presence of weak conditions $N_{ini}(x)$, $N_{up}(t)$ and $N_{down}(t)$, the Lax-Hopf formula (3.10) can be instantiated as follows.

Theorem 3.4. (Lax-Hopf formula with weak initial and boundary conditions) Consider the Hamilton Jacobi equation (3.9) with a continuous, concave Hamiltonian $f(\cdot)$, and define $v \doteq f'(0+)$, $-w \doteq f'(\rho_j-)$. Given weak conditions $N_{ini}(x)$, $N_{up}(t)$ and $N_{down}(t)$, the viability episolution given by (3.10) can be explicitly expressed as

$$N(t, x) = \min_{u \in [-w, v]} A(u; t, x) \quad (t, x) \in \Omega_I \quad (3.13)$$

$$N(t, x) = \min \left\{ \min_{u \in [\frac{x-a}{T}, v]} B(u; t, x), \min_{u \in [-w, \frac{x-a}{T}]} A(u; t, x) \right\} \quad (t, x) \in \Omega_{II} \quad (3.14)$$

$$N(t, x) = \min \left\{ \min_{u \in [\frac{x-b}{T}, v]} A(u; t, x), \min_{u \in [-w, \frac{x-b}{T}]} C(u; t, x) \right\} \quad (t, x) \in \Omega_{III} \quad (3.15)$$

$$N(t, x) = \min \left\{ \min_{u \in [\frac{x-a}{T}, v]} B(u; t, x), \min_{u \in [-w, \frac{x-b}{T}]} C(u; t, x), \min_{u \in [\frac{x-b}{T}, \frac{x-a}{T}]} A(u; t, x) \right\} \quad (t, x) \in \Omega_{IV} \quad (3.16)$$

where

$$A(u; t, x) = N_{ini}(x - ut) + tf^*(u) \quad (3.17)$$

$$B(u; t, x) = N_{up} \left(t - \frac{x-a}{u} \right) + \frac{x-a}{u} f^*(u) \quad (3.18)$$

$$C(u; t, x) = N_{down} \left(t - \frac{x-b}{u} \right) + \frac{x-b}{u} f^*(u) \quad (3.19)$$

and

$$\begin{aligned} \Omega_I &= \{(t, x) \in [0, T] \times [a, b] : x \geq a + vt, x \leq b - wt\} \\ \Omega_{II} &= \{(t, x) \in (0, T] \times [a, b] : x < a + vt, x \leq b - wt\} \\ \Omega_{III} &= \{(t, x) \in (0, T] \times [a, b] : x \geq a + vt, x > b - wt\} \\ \Omega_{IV} &= \{(t, x) \in (0, T] \times [a, b] : x < a + vt, x > b - wt\} \end{aligned} \quad (3.20)$$

Proof. The speeds of the kinematic waves fall within the interval $[-w, v]$, thus the temporal-spatial domain $[0, T] \times [a, b]$ can be partitioned into four parts, depending on whether or not a point (t, x) can be influenced by the initial, upstream boundary, and downstream boundary conditions; see Figure 2 for an illustration. To establish (3.13)-(3.16), it suffices, for each subregion, to locate the domain of influence and apply the Lax-Hopf formula (3.10). \square

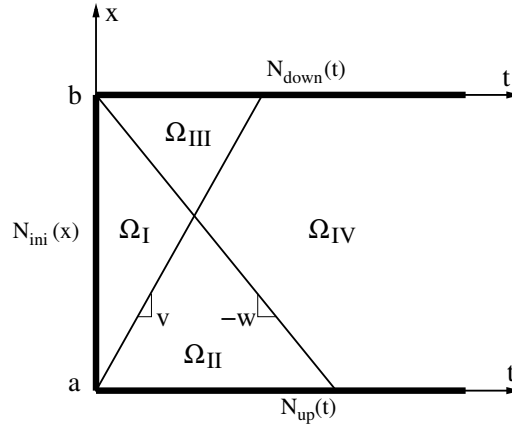


Figure 2: Partition of the temporal-spatial domain into four subregions. In Ω_I , the solution is influenced by $N_{ini}(\cdot)$ only; in Ω_{II} , the solution is influenced by $N_{up}(\cdot)$ and $N_{ini}(\cdot)$ only; in Ω_{III} , the solution is influenced by $N_{down}(\cdot)$ and $N_{ini}(\cdot)$; and in Ω_{IV} , the solution is influenced by $N_{ini}(\cdot)$, $N_{up}(\cdot)$ and $N_{down}(\cdot)$.

In view of the signalized junction in Figure 1 and the two signal models expressed in (2.7) and (2.8), we define the weak downstream boundary conditions for the H-J equation on link I_1 respectively as

$$N_{down}^{\Delta_A}(t) \doteq \int_0^t \mathcal{S}_3^1(\tau) u_1(\tau) d\tau \quad (\text{the on-and-off case}) \quad (3.21)$$

and

$$N_{down}^0(t) \doteq \int_0^t \eta_1 \mathcal{S}_3^1(\tau) d\tau \quad (\text{the continuum case}) \quad (3.22)$$

4. Convergence results and error estimation in the absence of spillback

In this section, under the assumption that no spillback occurs at the signalized junction, we are interested in finding out the asymptotic behavior of the on-and-off signal model, and whether or not it converges to the continuum model, when the signal cycle length tends to zero. As we shall explain, the no-spillback assumption is crucial for the established results below. The case with spillback will be presented later in Section 5. Note that all the results presented in the rest of this section are valid for any type of fundamental diagram as long as the very mild assumptions (F) mentioned in the introduction are satisfied.

4.1. Convergence result without spillback

Let us re-visit the merge junction A depicted in Figure 1. The absence of spillback at node A implies that the entrance of link I_3 remains in the uncongested phase. In other words, the supply function $\mathcal{S}_3(t)$ of I_3 is equal to its flow capacity. The following convergence theorem holds under such circumstance.

Theorem 4.1. Consider the merge junction depicted in Figure 1, and a signal control $u_1(t)$ for link I_1 with cycle Δ_A and split parameter $\eta_1 \in (0, 1)$. We let $N_{up}(t)$ and $N_{ini}(x)$ be the weak upstream boundary condition and initial condition for the H-J equation (3.9) on I_1 . Let

$N^{\Delta_A}(t, x)$ and $N^0(t, x)$ be the solutions of the H-J equation with additional downstream boundary conditions $N_{down}^{\Delta_A}(t)$ and $N_{down}^0(t)$ respectively, where $N_{down}^{\Delta_A}(t)$ and $N_{down}^0(t)$ are given by (3.21) and (3.22). Furthermore, assume that the entrance of link I_3 remains in the uncongested phase. Then $N^{\Delta_A}(t, x) \rightarrow N^0(t, x)$ uniformly for all $(t, x) \in [0, T] \times [a_1, b_1]$, as $\Delta_A \rightarrow 0$.

Proof. We readily notice that the control function $u_1(t)$ defined in (2.5) converges weakly to the constant function η_1 on the time interval $[0, T]$ as $\Delta_A \rightarrow 0$. According to the no-spillback hypothesis, the effective supply $S_3^1(t) \doteq \min\{C_1, S_3(t)\} \equiv \min\{C_1, C_3\}$ where C_3 denotes the flow capacity of I_3 . Therefore by the definition of weak convergence, we have

$$N_{down}^{\Delta_A}(t) = \int_0^t S_3^1(\tau) u_1(\tau) d\tau \rightarrow \int_0^t \eta_1 S_3^1(\tau) d\tau = N_{down}^0(t) \quad \text{as } \Delta_A \rightarrow 0 \quad (4.23)$$

uniformly for all $t \in [0, T]$.

By (3.13) and (3.14), we deduce that $N^{\Delta_A}(t, x) \equiv N^0(t, x)$ for all $(t, x) \in \Omega_I \cup \Omega_{II}$, since the solution in these regions is not affected by the downstream boundary condition.

We next turn our attention to region $\Omega_{III} \cup \Omega_{IV}$. Given any $\varepsilon > 0$, by virtue of (4.23), there exists a $\delta > 0$ such that whenever $\Delta_A < \delta$, we have

$$|N_{down}^{\Delta_A}(t) - N_{down}^0(t)| < \varepsilon \quad \forall t \in [0, T] \quad (4.24)$$

Fix arbitrary $(t, x) \in \Omega_{III} \cup \Omega_{IV}$, we denote

$$u^{*,\Delta_A} \doteq \operatorname{argmin}_{u \in [-w, \frac{x-b}{t}]} \left\{ N_{down}^{\Delta_A} \left(t - \frac{x-b}{u} \right) + \frac{x-b}{u} f^*(u) \right\} \quad (4.25)$$

$$u^{*,0} \doteq \operatorname{argmin}_{u \in [-w, \frac{x-b}{t}]} \left\{ N_{down}^0 \left(t - \frac{x-b}{u} \right) + \frac{x-b}{u} f^*(u) \right\} \quad (4.26)$$

According to (4.24) and (4.26),

$$\begin{aligned} N_{down}^{\Delta_A} \left(t - \frac{x-b}{u^{*,\Delta_A}} \right) + \frac{x-b}{u^{*,\Delta_A}} f^*(u^{*,\Delta_A}) &\geq N_{down}^0 \left(t - \frac{x-b}{u^{*,\Delta_A}} \right) + \frac{x-b}{u^{*,\Delta_A}} f^*(u^{*,\Delta_A}) - \varepsilon \\ &\geq N_{down}^0 \left(t - \frac{x-b}{u^{*,0}} \right) + \frac{x-b}{u^{*,0}} f^*(u^{*,0}) - \varepsilon \end{aligned}$$

We may similarly deduce from (4.24) and (4.25) that

$$N_{down}^0 \left(t - \frac{x-b}{u^{*,0}} \right) + \frac{x-b}{u^{*,0}} f^*(u^{*,0}) \geq N_{down}^{\Delta_A} \left(t - \frac{x-b}{u^{*,\Delta_A}} \right) + \frac{x-b}{u^{*,\Delta_A}} f^*(u^{*,\Delta_A}) - \varepsilon$$

Thus

$$\left| \min_{u \in [-w, \frac{x-b}{t}]} \left\{ N_{down}^{\Delta_A} \left(t - \frac{x-b}{u} \right) + \frac{x-b}{u} f^*(u) \right\} - \min_{u \in [-w, \frac{x-b}{t}]} \left\{ N_{down}^0 \left(t - \frac{x-b}{u} \right) + \frac{x-b}{u} f^*(u) \right\} \right| < \varepsilon \quad (4.27)$$

In view of (3.15) and (3.16), the above estimate gives the difference in $\min_{u \in [-w, \frac{x-b}{t}]} C(u; t, x)$ when $N_{down}^{\Delta_A}(\cdot)$ and $N_{down}^0(\cdot)$ are respectively used. Since the rest of the quantities appearing in (3.15)-(3.16) do not depend on the downstream boundary condition, we conclude that $|N^{\Delta_A}(t, x) - N^0(t, x)| < \varepsilon$ for all $(t, x) \in \Omega_{III} \cup \Omega_{IV}$. This implies the desired uniform convergence. \square

Remark 4.2. One important observation from the proof of Theorem 4.1 is that when conditions $N_{ini}(x)$ and $N_{up}(t)$ are fixed, the difference of the two Moskowitz functions $|N^{\Delta A}(t, x) - N^0(t, x)|$ is bounded by the maximum difference of their respective weak downstream boundary conditions, that is,

$$|N^{\Delta A}(t, x) - N^0(t, x)| \leq \max_{\tau \in [0, t]} |N_{down}^{\Delta A}(\tau) - N_{down}^0(\tau)| \quad \forall t \in [0, T], \quad x \in [a, b]$$

In other words, approximation of the Moskowitz function is only “as good as” how $N_{down}^{\Delta A}(t)$ is approximated by $N_{down}^0(t)$. Such insight is crucial for our error analysis presented later.

The next corollary generalizes the convergence result stated for a single junction to a network.

Corollary 4.3. Consider a network with a fixed-cycle-and-split signal control at each intersection, with merge rules given by (2.7). Assume the flow dynamic on each link is governed by a scalar conservation law (1.1) with a continuous and concave fundamental diagram. In addition, assume that the entrance of every link remains in the uncongested phase; i.e., no spillback occurs in the network. Then the solution on this network converges to the one corresponding to the continuum signal model (2.8), when the traffic signal cycles tend to zero.

Proof. Without loss of generality we assume that the network is initially empty. Under the stated hypothesis, for each link, the supply function of this link is always a constant and equal to its flow capacity. According to Theorem 4.1, convergence to a continuum model holds at each signalized intersection. Further notice that the error of the continuum approximation (2.8) on each link adds up linearly throughout the network. Thus the convergence also holds on a network level. \square

4.2. Approximation errors without spillback

In the previous section, we have established convergence results for the continuum signal models in regimes where the signal cycles are infinitesimal. While providing theoretical foundations for a class of approximate signalized junction models, these convergence results are not satisfying from a practical point of view since any signal cycle must be bounded away from zero. To make our investigations more practical, we conduct further analysis on the approximation error of the continuum model when the cycles are not infinitesimal. Results presented below may assist practitioners with applying the continuum approximation of the on-and-off signal models and evaluating its efficacy.

Theorem 4.4. (Error estimate without spillback) Consider the signalized merge junction depicted in Figure 1. Assume the Hamilton-Jacobi equation (3.9) for link I_1 has weak value conditions $N_{ini}(x)$ and $N_{up}(t)$. Furthermore, let $N^{\Delta A}(t, x)$ and $N^0(t, x)$ be the solutions of this H-J equation with additional downstream boundary conditions $N_{down}^{\Delta A}(t)$ and $N_{down}^0(t)$ respectively, where $N_{down}^{\Delta A}(t)$ and $N_{down}^0(t)$ are given in (3.21) and (3.22). In addition, assume that the entrance of link I_3 remains in the uncongested phase. Then for all $(t, x) \in [0, T] \times [a_1, b_1]$,

$$|N^{\Delta A}(t, x) - N^0(t, x)| \leq \eta_1(1 - \eta_1)\Delta_A \min\{C_1, C_3\} \leq \frac{1}{4}\Delta_A \min\{C_1, C_3\} \quad (4.28)$$

Proof. According to the hypothesis, we have that $\mathcal{S}_3^1(t) \equiv \min\{C_1, C_3\}$. Then for any $t \geq 0$,

$$|N_{down}^{\Delta A}(t) - N_{down}^0(t)| = \min\{C_1, C_3\} \left| \int_0^t u_1(\tau) d\tau - \eta_1 t \right| \leq \eta_1(1 - \eta_1)\Delta_A \min\{C_1, C_3\} \quad (4.29)$$

Therefore, using the same argument as in the proof of Theorem 4.1, we conclude that

$$|N^{\Delta_A}(t, x) - N^0(t, x)| \leq \max_{\tau \in [0, t]} |N_{down}^{\Delta_A}(\tau) - N_{down}^0(\tau)| \leq \eta_1(1 - \eta_1)\Delta_A \min\{C_1, C_3\}$$

for all $(t, x) \in [0, T] \times [a_1, b_1]$. Finally, it is useful to notice that $\eta_1(1 - \eta_1) \leq \frac{1}{4}$, and the equality holds if and only if $\eta_1 = \frac{1}{2}$. \square

In parallel to Section 4.1, we state the error estimates for a whole network in the corollary below.

Corollary 4.5. *Consider a network with a fixed-cycle signal control at each intersection, with merge rules given by (2.7). Assume the flow dynamic on each link is governed by a scalar conservation law (1.1) with a continuous and concave fundamental diagram. In addition, assume that the entrance of every link remains in the uncongested phase. Then for every link I_i of the network, let $N^{\Delta_i}(t, x)$ and $N^{0,i}(t, x)$ be the two Moskowitz functions obtained from the on-and-off and the continuum modeling approaches respectively. Then $|N^{\Delta_i}(t, x) - N^{0,i}(t, x)|$ is less than or equal to the sum of such differences of preceding links including I_i .*

Proof. Without loss of generality, we again assume that the network is initially empty. If the upstream condition $N_{up}^i(t)$ of I_i is fixed, the error $|N^{\Delta_i}(t, x) - N^{0,i}(t, x)|$ is estimated by (4.28). However, $N_{up}^i(t)$ may be subject to errors due to the continuum signal approximations on the preceding links. Clearly such error adds up linearly throughout the network, therefore the actual $|N^{\Delta_i}(t, x) - N^{0,i}(t, x)|$ is bounded by a summation of errors from previous links. \square

Remark 4.6. *The error estimation established in Corollary 4.5 is quite conservative in that it assumes the worst case scenario where errors add up without cancellation. In order to obtain a more accurate estimation, one needs to look at specific network topology and the actual signal split and cycles used, including the initial phase of each signal. The key message from Corollary 4.5 is that the continuum approximation picks up errors from one link to another additively at the most.*

5. Convergence results and error estimation in the presence of spillback

In the previous section, asymptotic behavior of the on-and-off signal model as well as the approximation error of its continuum counterpart are investigated under the assumption that the entrance of I_3 remains in the uncongested phase. On the other hand, if I_3 is dominated by the congested phase, the signal control $u_3(t)$ located at node B may directly affect supply $S_3(t)$ and hence $S_3^1(t)$. As we shall explain below, when this happens the previously stated convergence result and error estimation no longer hold in certain cases, depending on the type of fundamental diagram employed.

For the remainder of this section, we will examine the behavior of the continuum approximation model assuming that spillback persists for a significant period of time (i.e., for at least several signal cycles). The case where spillback persists for a much shorter period of time will be discussed in Section 6.

5.1. Convergence result with spillback

5.1.1. The case with triangular fundamental diagram

We will first demonstrate analytically that the convergence does not hold with vehicle spillback if a triangular fundamental diagram is assumed. A triangular fundamental diagram has the following form:

$$f(\rho) = \begin{cases} v\rho & \rho \in [0, \rho_c] \\ -w(\rho - \rho_j) & \rho \in (\rho_c, \rho_j] \end{cases} \quad (5.30)$$

where v and w are the speeds of the forward- and backward-propagating kinematic waves respectively. In the case of triangular fundamental diagram, v also coincides with the free-flow speed. ρ_c denotes the critical density, and ρ_j denotes the jam density.

Consider the merge junction in Figure 1. Let us focus on I_3 which remains in the congested phase. In the spatial-temporal domain of I_3 , characteristic lines with slope $-w_3$ emit from the right boundary $x = b_3$ and reach the left boundary $x = a_3$, where w_3 denotes the backward wave speed on link I_3 (see Figure 3). When the light is red, the exit flow q_3 is equal to zero, creating a kinematic wave with speed $-w_3$ and density value ρ_j^3 where ρ_j^3 denotes the jam density of I_3 ; when the light is green, the exit flow q_3 is equal to the flow capacity C_3 , creating a kinematic wave with speed $-w_3$ and density value ρ_c^3 , where ρ_c^3 denotes the critical density on I_3 . As a result, the supply function $S_3(t)$ at the entrance of I_3 fluctuates between 0 and C_3 , leading $S_3^1(t)$ to fluctuate between 0 and $\min\{C_1, C_3\}$.

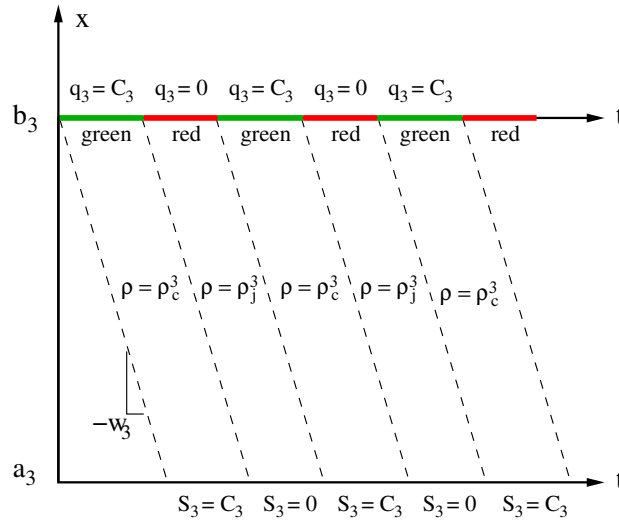


Figure 3: The scenario where link I_3 is in the congested phase, when a triangular fundamental diagram is employed. The dashed lines represent characteristics traveling backward at speed w_3 . C_3 denotes the flow capacity; q_3 denotes the link exit flow; ρ_c^3 and ρ_j^3 denote the critical density and the jam density respectively; S_3 denotes the supply at the entrance of the link.

The key observation is that the effective supply $S_3^1(t)$ does not have bounded variation as the signal cycle of $u_3(t)$ tends to zero. As a consequence, the convergence expressed in (4.23) no longer holds. To see this, we simply adjust u_1 and u_3 such that $S_3(t) = C_3 \cdot u_1(t)$ (in this case, we

say that signal controls u_1 and u_3 are resonant) and perform the following calculation:

$$\int_0^t \mathcal{S}_3^1(\tau) u_1(\tau) d\tau = \int_0^t \min\{C_1, C_3\} \cdot u_1^2(\tau) d\tau = \int_0^t \min\{C_1, C_3\} \cdot u_1(\tau) d\tau = \int_0^t \mathcal{S}_3^1(\tau) d\tau$$

which never converges to $\eta_1 \int_0^t \mathcal{S}_3^1(\tau) d\tau$ regardless of the cycle length Δ_A . Even if u_1 and u_3 are not resonant, due to the fact that $\mathcal{S}_3^1(t)$ does not have bounded variation as the cycle of $u_3(t)$ becomes smaller and smaller, the convergence will not hold in general (in fact, $\mathcal{S}_3^1(t)$ will oscillate more and more violently as the cycle of $u_3(t)$ diminishes). We thus conclude that in the case of a triangular fundamental diagram, the proposed continuum junction model does not yield a sound approximation of networks controlled by more than one on-and-off signal lights, unless the spillback case depicted in Figure 3 does not occur.

5.1.2. The case with strictly concave fundamental diagram

This section establishes convergence result for the on-and-off signal model with strictly concave fundamental diagram. A strictly concave fundamental diagram $f(\cdot)$ is a piecewise smooth function that satisfies, in addition to **(F)**,

$$f''(\rho) \leq -b \quad \text{for some } b > 0 \quad (5.31)$$

for all $\rho \in [0, \rho_j]$ such that $f(\cdot)$ is twice differentiable at ρ .

Let us re-visit the scenario where link I_3 is dominated by the congested phase, but now assume a strictly concave fundamental diagram. We begin with the observation that in this case the characteristic field is genuinely nonlinear. As a result, any flux variation generated by signal control at the exit of the link gets instantaneously reduced when the waves propagate backwards, see Bressan (2000) for more mathematical details. Therefore, it is expected that the convergence may still hold even in the presence of spillback. The following lemma is the key ingredient of our convergence result and its proof is quite informative.

Lemma 5.1. *Given the merge junction in Figure 1, we focus on the link I_3 expressed as a spatial interval $[0, L]$ with a strictly concave fundamental diagram $f(\cdot)$. Assume that a signal control $u_3(t)$ with a fixed cycle-and-split is present at the exit of I_3 (node B) and that the whole link I_3 remains in the congested phase. Then the supply function $S_3(t)$ converges to some constant S_3^* uniformly as the cycle length of $u_3(t)$ tends to zero.*

Proof. The proof is divided into several parts.

Part 1. We begin by noticing that when I_3 is in the congested phase, in the presence of alternating phases of red and green at the downstream boundary of I_3 , the density profile on this congested link consists of shock and rarefaction waves. As Part I of Figure 4 shows, during the green time, a rarefaction wave is formed which then interacts with the characteristic lines generated by the red phase that comes afterwards. As a result of such interaction, a shock is formed which propagates backward until it reaches the entrance of I_3 ($x = 0$). It is quite obvious from Part I of Figure 4 that the flow variable at the entrance of I_3 , and hence the supply $S_3(t)$, will display a repeated pattern with downward jumps, which is illustrated in Part II of Figure 4. Therefore, to show the desired result it suffices to estimate the magnitude of such jumps using an Oleinik-type estimate, as follows.

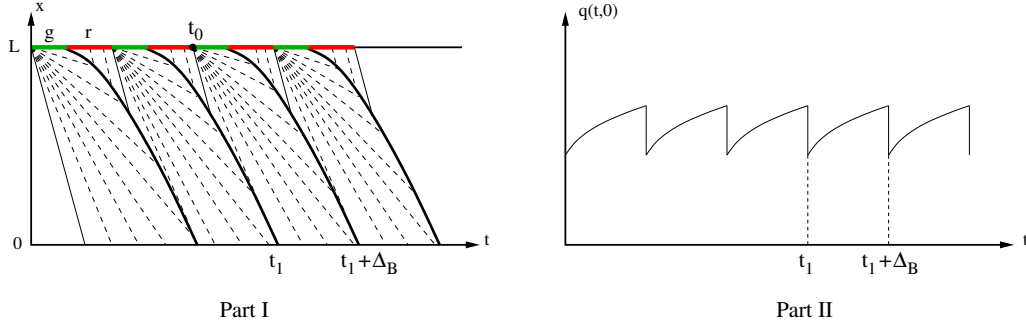


Figure 4: Link I_3 dominated by the congested phase. Left: the repeated pattern in the density profile is caused by the on-and-off signal at the downstream boundary. Right: the time-dependent flow variable (and also the supply $S_3(t)$) observed at the upstream boundary of I_3 .

Part 2. We readily notice that due to the prevailing congested phase, one can represent the dynamics with a scalar conservation law in the flow variable $q(t, x)$ instead of the density variable $\rho(t, x)$. In particular, we define

$$g(q) \doteq \max \{ \rho \in [0, \rho_j] : f(\rho) = q \} = \{ \rho \in [\rho_c, \rho_j] : f(\rho) = q \} \quad q \in [0, C] \quad (5.32)$$

which is the inverse of the fundamental diagram corresponding to the congested phase, where ρ_c denotes the unique critical density and C denotes the flow capacity. We introduce the conservation law with a downstream boundary condition

$$\begin{cases} \partial_x q(t, x) + \partial_t g(q(t, x)) = 0 & (t, x) \in [0, T] \times [0, L] \\ q(t, L) = q_{exit}(t) \end{cases} \quad (5.33)$$

where $q(t, x)$ denotes the flow at a point in the temporal-spatial domain, $q_{exit}(t)$ denotes the link exit flow which is determined by the signal control $u_3(t)$. The conservation law in (5.33) is equivalent to (1.1) under the assumption that the link is dominated by the congested phase. A similar technique has been applied in Bressan and Han (2011), and the reader is referred to Friesz et al. (2013) for a proof of such equivalence. We further notice that by switching the roles of x and t , the downstream boundary condition $q_{exit}(t)$ can be viewed as a “terminal condition” for (5.33). Since the Oleinik estimate holds only in a time-forward fashion (Bressan, 2000), we introduce the dummy variable $y = -x$ and write

$$\partial_y q(t, -y) - \partial_t g(q(t, -y)) = 0 \quad (t, y) \in [0, T] \times [-L, 0] \quad (5.34)$$

with what is now the “initial condition”

$$q(t, -L) = q_{exit}(t) \quad (5.35)$$

For such an initial value problem (5.34)-(5.35), the standard Oleinik estimate holds, that is,

$$\partial_t q(t, -y) \leq \frac{-1}{c(L+y)}, \quad \text{or} \quad \partial_t q(t, x) \leq \frac{-1}{c(L-x)} \quad (5.36)$$

whenever $(t, -y)$ or (t, x) is away from shock waves, where $c < 0$ is any upper bound on $g''(\cdot)$.² The value of c can be determined as follows. In view of (5.32), we have for any $\rho \in [\rho_c, \rho_j]$ that

$$\begin{aligned} \rho \equiv g(f(\rho)) &\implies 0 = [g(f(\rho))]'' = g''(f(\rho))[f'(\rho)]^2 + g'(f(\rho))f''(\rho) \\ &\implies g''(f(\rho)) = -\frac{f''(\rho)}{[f'(\rho)]^3} \leq \frac{b}{[f'(\rho_j)]^3} \doteq c \end{aligned}$$

where b is given by (5.31). Notice that we used the identity $g'(f(\rho)) \cdot f'(\rho) = 1$ in the above deduction. Setting $x = 0$, the Oleinik estimate (5.36) yields the following critical result on the gradient of the flux at the entrance of I_3 :

$$\partial_t q(t, 0) \leq -\frac{[f'(\rho_j)]^3}{bL} \quad (5.37)$$

Part 3. We are now in a position ready to estimate the magnitude of the downward jumps depicted in Part II of Figure 4. To do so, we readily notice that the duration between two consecutive jumps is comparable to a cycle length Δ_B . Thus the magnitude of the jump is bounded by

$$\Delta_B \cdot \frac{-[f'(\rho_j)]^3}{bL} \quad (5.38)$$

which tends to zero as the cycle length goes to zero. We thus conclude that the flow $q(t, 0)$, and hence the supply $S_3(t)$ converges to a constant uniformly as $\Delta_B \rightarrow 0$. \square

Remark 5.2. *In contrast to the triangular case, the convergence result holds for the strictly concave case even in the presence of vehicle spillback. An intuitive explanation, as we mention before, is related to the nonlinear effect caused by the strictly concave fundamental diagram. Figure 5 compares the supply profiles observed at the entrance of link I_3 when the whole link is in the congested phase. As $\Delta_B \rightarrow 0$, in the triangular case the oscillation in $S_3(t)$ has the biggest amplitude and becomes more and more frequent, causing the total variation to blow up and the convergence (4.23) to fail. On the other hand, in the strictly concave case the oscillation in $S_3(t)$ is damped as it gets more and more frequent. In fact, one may easily show by (5.38) that the supply $S_3(t)$ has uniform bounded variation regardless of the cycle length Δ_B . Thus the convergence (4.23) continues to hold in this case.*

We are now in a position ready to state and prove the convergence result for the strictly concave case.

Theorem 5.3. *Consider a network with a fixed-cycle-and-split signal control at each node, where the flow dynamic on each link is governed by a Hamilton-Jacobi equation (3.9) with a strictly concave fundamental diagram. We further assume that the entrance of each link may remain in the congested phase for some period of time, which spans at least several signal cycles. Then the solution of this network converges to the one corresponding to the continuum signal model, when the traffic signal cycles tend to zero.*

²Notice that the estimate (5.36) holds true for any downstream condition $q_{exit}(t)$.

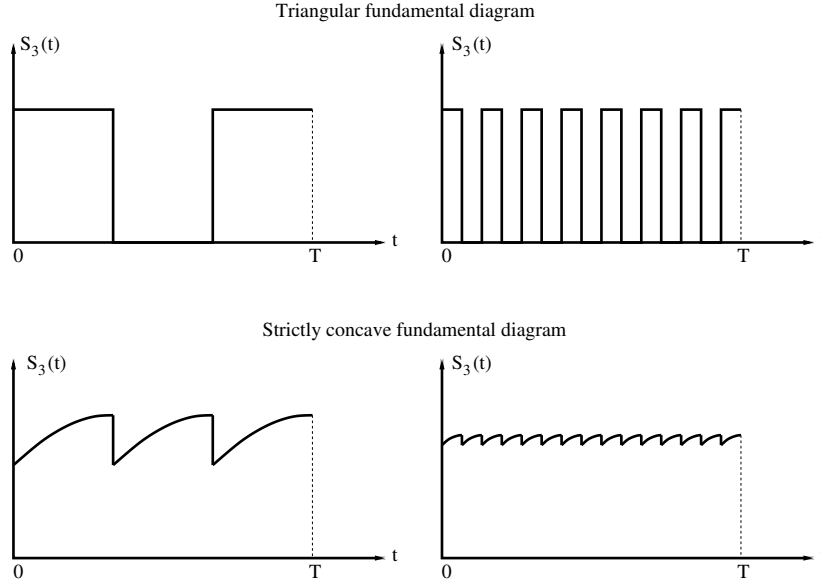


Figure 5: Profiles of the supply observed at the entrance of I_3 , when I_3 is dominated by the congested phase and controlled by a signal $u_3(t)$ at the exit. First row: the triangular case; second row: the strictly concave case. First column: larger signal cycle; second column: smaller signal cycle.

Proof. For the junction depicted in Figure 1, if the entrance of I_3 is in the uncongested phase, the convergence is proven in Theorem 4.1. If I_3 is dominated by the congested phase, Lemma 5.1 asserts that $S_3(t)$ converges to some $S_3^*(t)$ uniformly and in the L^2 -norm as $\Delta_B \rightarrow 0$, which implies the same convergence $S_3^1(t) \rightarrow S_3^{1,*}(t)$, where $S_3^1(t) = \min\{C_1, S_3(t)\}$, $S_3^{1,*}(t) = \min\{C_1, S_3^*(t)\}$. Thus we have

$$\int_0^t S_3^1(\tau) u_1(\tau) d\tau \rightarrow \eta_1 \int_0^t S_3^{1,*}(\tau) d\tau, \quad \text{as } \Delta_A \rightarrow 0$$

uniformly for all $t \in [0, T]$. We then apply a proof similar to that in Theorem 4.1 and conclude the Moskowitz function $N^{\Delta_A}(t, x)$ converges to $N^0(t, x)$ on I_1 as $\Delta_A \rightarrow 0$.

Finally, notice that the approximation error of the continuum model adds up linearly through the network, thus such convergence holds on the whole network. \square

5.2. Approximation errors with spillback

This section is devoted to establishing the approximation error of the continuum signal model when the signal cycles in the on-and-off model are not infinitesimal, and when spillback occurs at the intersection. In contrast to the non-spillback case, the difference between the two models in the presence of spillback may be larger and grow with time.

Let us recall the signalized merge junction shown in Figure 1, and focus on the link I_1 . All notations employed earlier will remain in effect in this section.

Theorem 5.4. (Error estimate with spillback) *Under the same setting and notations of Theorem 4.4, we assume that the entrance of link I_3 may remain in the congested phase for some*

period of time, which spans at least several signal cycles. Then if the Hamiltonian is triangular,

$$|N^{\Delta_A}(t, x) - N^0(t, x)| \leq \eta_1(1 - \eta_1)\Delta_A \min\{C_1, C_3\} + \min\{C_1, C_3\} \eta_1 t \quad (5.39)$$

where C_1 and C_3 denotes the flow capacity of link I_1 and I_3 respectively. If the Hamiltonian is strictly concave,

$$|N^{\Delta_A}(t, x) - N^0(t, x)| \leq \eta_1(1 - \eta_1)\Delta_A \min\{C_1, C_3\} + \min\left\{C_1, f\left((f')^{-1}\left(\frac{-L}{L/w + \Delta_B}\right)\right)\right\} \eta_1 t \quad (5.40)$$

for all $(t, x) \in [0, T] \times [a_1, b_1]$, where Δ_B denotes the cycle length of signal $u_3(t)$ located at the downstream boundary of I_3 , $f(\cdot)$ denotes the strictly concave fundamental diagram of I_3 with $f'(\rho_j) = -w$, ρ_j and L denotes the jam density and the length of I_3 respectively.

Remark 5.5. In case $f(\cdot)$ is not continuously differentiable at some ρ_1 and $f'(\rho_1^-) > \frac{-L}{L/w + \Delta_B} > f'(\rho_1^+)$, then we set

$$(f')^{-1}\left(\frac{-L}{L/w + \Delta_B}\right) = \rho_1$$

The conclusion of Theorem 5.4 still holds.

Proof. Case 1. (Triangular Hamiltonian) When the entrance of link I_3 becomes congested, the scenario described in Figure 3 occurs. As a result, the supply function $S_3(t) \in \{0, C_3\}$, which implies that $S_3^1(t) \in \{0, \min\{C_1, C_3\}\}$. Therefore for any $t \gg \Delta_A$,

$$0 \leq N_{down}^{\Delta_A}(t) = \int_0^t S_3^1(\tau) \cdot u_1(\tau) d\tau \leq \min\{C_1, C_3\} \int_0^t u_1(\tau) d\tau \approx \min\{C_1, C_3\} \eta_1 t$$

$$0 \leq N_{down}^0(t) = \int_0^t \eta_1 S_3^1(\tau) d\tau \leq \min\{C_1, C_3\} \int_0^t \eta_1 d\tau = \min\{C_1, C_3\} \eta_1 t$$

And we have that

$$|N_{down}^{\Delta_A}(t) - N_{down}^0(t)| \leq \min\{C_1, C_3\} \eta_1 t$$

Whenever the entrance of I_3 becomes uncongested, the additional difference between $N_{down}^{\Delta_A}(t)$ and $N_{down}^0(t)$ is always bounded by $\eta_1(1 - \eta_1)\Delta_A \min\{C_1, C_3\}$ and independent of time, as we have shown in Theorem 4.4. For any $t \in [0, T]$ we deduce, in the same way as in Theorem 4.1, that

$$|N^{\Delta_A}(t, x) - N^0(t, x)| \leq \max_{\tau \in [0, t]} |N_{down}^{\Delta_A}(\tau) - N_{down}^0(\tau)| \leq (\eta_1(1 - \eta_1)\Delta_A + \eta_1 t) \min\{C_1, C_3\}$$

Case 2. (Strictly concave Hamiltonian) When the entrance of link I_3 is in the congested phase, our calculation in the proof of Lemma 5.1 shows that the density profile at the entrance of I_3 consists of shocks and rarefaction waves. In order to establish a close estimate of the magnitude of the jumps depicted in Part II of Figure 4, we notice that the duration between two consecutive jumps is approximately Δ_B . Define $[t_1, t_1 + \Delta_B]$ to be the time interval between two consecutive jumps; then we have $t_1 \geq t_0 + L/w$ where t_0 denotes the time at which this rarefaction emerges. See Part I of Figure 4 for an illustration. Note that for every $t \in [t_0 + L/w, t_1 + \Delta_B]$ the map $t \mapsto f\left((f')^{-1}\left(\frac{L}{t-t_0}\right)\right)$, which is given by the rarefaction wave, is a concave function in t . We

deduce that

$$\underbrace{f\left((f')^{-1}\left(\frac{-L}{t_1 + \Delta_B - t_0}\right)\right)}_X - \underbrace{f\left((f')^{-1}\left(\frac{-L}{t_1 - t_0}\right)\right)}_Y \leq f\left((f')^{-1}\left(\frac{-L}{L/w + \Delta_B}\right)\right) - f\left((f')^{-1}\left(\frac{-L}{L/w}\right)\right) \quad (5.41)$$

$$= f\left((f')^{-1}\left(\frac{-L}{L/w + \Delta_B}\right)\right) \quad (5.42)$$

Inequality (5.41) is due to concavity and the fact that $t_1 + \Delta_B - t_0 \geq L/w + \Delta_B$. Notice that X and Y from (5.41) are precisely the maximum and minimum of the flow variable $q(t, 0)$ inside the time interval $[t_1, t_1 + \Delta_B]$. Thus (5.42) provides an upper bound on the jumps in flow and in the supply function $S_3(t)$.

Since $Y \leq S_3(t) \leq X$, we have that $\min\{C_1, Y\} \leq S_3^1(t) \leq \min\{C_1, X\}$. Similar to **Case 1**, we have the following estimates

$$\min\{C_1, Y\} \eta_1 t \leq \int_0^t S_3^1(\tau) \cdot u(\tau) d\tau \leq \min\{C_1, X\} \eta_1 t \quad (5.43)$$

$$\min\{C_1, Y\} \eta_1 t \leq \int_0^t \eta_1 S_3^1(\tau) d\tau \leq \min\{C_1, X\} \eta_1 t \quad (5.44)$$

so

$$\begin{aligned} |N_{down}^{\Delta_A}(t) - N_{down}^0(t)| &\leq \max_{\tau \in [0, t]} \left| \int_0^t S_3^1(\tau) \cdot u(\tau) d\tau - \int_0^t \eta_1 S_3^1(\tau) d\tau \right| \\ &\leq (\min\{C_1, X\} - \min\{C_1, Y\}) \eta_1 t \leq \min\{C_1, X - Y\} \eta_1 t \\ &\leq \min\left\{C_1, f\left((f')^{-1}\left(\frac{-L}{L/w + \Delta_B}\right)\right)\right\} \eta_1 t \end{aligned} \quad (5.45)$$

Again, an additional term $\eta_1(1 - \eta_1)\Delta_A \min\{C_1, C_3\}$ is attached to the error when the entrance of I_3 is in the uncongested phase. This establishes (5.40). \square

Notice that in the presence of spillback, the errors associated with triangular or strictly concave fundamental diagrams both grow with time. However, the error in the strictly concave case is much smaller than the triangular case. This is quite clear from Remark 5.2 and will be numerically verified later in Section 7. Inequalities (4.28), (5.39) and (5.40) are three of the most significant expressions in this paper, as they not only provide comprehensive error estimates, but also explain the convergence/non-convergence we established earlier when the signal cycles tend to zero: that is, by setting $\Delta_A \rightarrow 0$, $\Delta_B \rightarrow 0$, the right hand side of (5.40) tends to zero, while the right hand side of (5.39) does not.

Remark 5.6. *The different errors associated with the triangular (not strictly concave) fundamental diagram and the strictly concave one can be interpreted in prose as follows: the more concave a fundamental diagram is, the more nonlinear its characteristic field is, and the more cancellation to the flow variation it causes, hence the less error we find in the approximation. Notice that when $f(\cdot)$ is twice differentiable, the error estimates can be stated in terms of the second derivative using the same Oleinik-type estimate as we did in Lemma 5.1, that is, the*

magnitude of the oscillation in supply $S_3(t)$ in the presence of spillback is bounded by

$$\Delta_B \cdot \frac{-[f'(\rho_j)]^3}{bL} \quad (5.46)$$

such quantity is directly related to the approximation error. Recall that the constant b is such that $f''(\rho) \leq -b, \forall \rho$; thus it is a direct indicator of how concave the fundamental diagram is. In particular, if $f(\cdot)$ is triangular, then $b = 0$ and the quantity (5.46) blows up, resulting in the maximum error possible. Such interpretation using the second derivative provides further insight into the importance of strict concavity in reducing the approximation error.

6. Continuum approximation in the presence of transient spillback

In the previous two sections, we have considered the case with and without spillbacks. In both cases, it is assumed that the uncongested phase or the congested phase persists at the entrance of link I_3 for a significant period of time, usually on the scale of several signal cycles. Such assumption is crucial for our analysis since the continuum signal model is one type of aggregate models which approximates the cumulative throughput of a signalized junction within at least one full signal cycle. If the spillback/non-spillback state of the system fluctuates on a much smaller time scale, say shorter than a full cycle, then the previously established convergence and error estimates may not hold. We will refer to such situation as *transient spillback*.

Let us illustrate the impact of transient spillback on the approximating quality of the continuum signal model using a specific example. Consider the three-incoming, one-outgoing signal junction shown in Figure 6. Assume vehicles flow into links a_1 and a_3 with the maximum rate (flow capacity), while link a_2 remains empty. Let a_4 be congested. In addition, assign equal signal split of $1/3$ to each incoming link. We also stipulate that the sequence of links allowed to enter a_4 is $a_1, a_2, a_3, a_1, a_2, a_3 \dots$

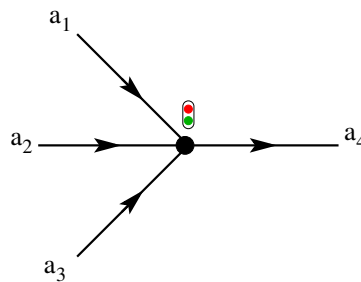


Figure 6: The signalized junction with three incoming links and one outgoing link.

In an on-and-off scenario, when the light for a_1 is green, the supply from downstream is limited since a_4 is in the congested phase. On the other hand, when the light turns green for a_3 , due to the previous green phase for the empty link a_2 which allows the entrance of a_4 to clear up a little bit, the supply from a_4 will be maximum and equal to its flow capacity. When vehicles from a_3 fill up this empty space on link a_4 , vehicles from a_1 are once again faced with a limited downstream supply. Therefore, it is reasonable to expect the throughputs of links a_1 and a_3 are quite different, despite the fact that they are assigned equal signal split. Such an asymmetric situation will persist even if signal cycles tend to zero.

A numerical simulation is conducted to confirm this observation. Figure 7 shows the throughputs (cumulative exiting vehicle curves) of links a_1 and a_3 , when then same signal split of $1/3$ is assigned to each approach. In these figures, the bifurcation point of the cumulative curves indicates the first time spillback occurs. We clearly observe that convergence of the on-and-off model to the continuum model does not hold, no matter how small the signal cycle is. Figure 8 shows the supply profiles on link a_4 , where we observe the predicted transient spillbacks (where the supply is lower). Such transient spillback resonates with the signal phases, causing links a_1 and a_3 to face completely different downstream supplies when their respective lights are green.

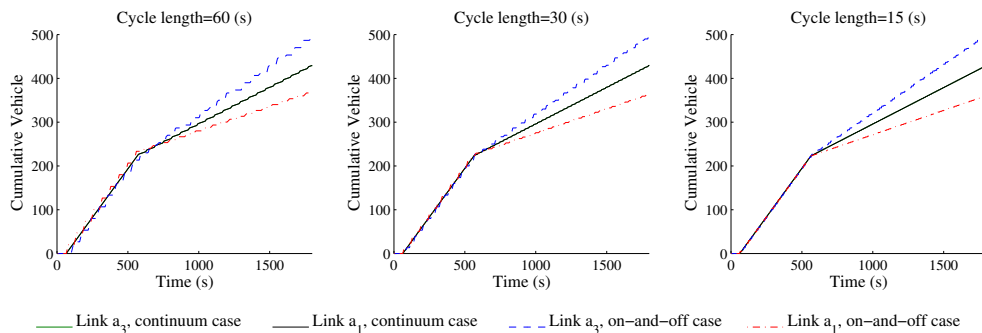


Figure 7: The cumulative exiting vehicle counts on links a_1 and a_3 , with the continuum model and the on-and-off model.

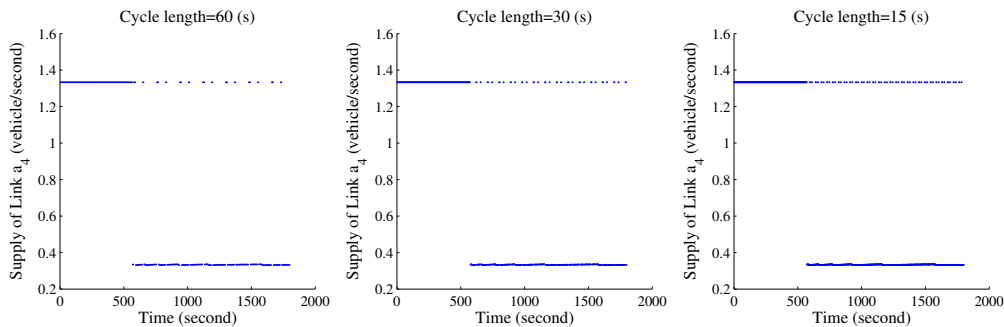


Figure 8: The supply functions of a_4 . The lower value (≈ 0.33) indicates the presence of spillback; the higher value ($= 4/3$), which is equal to the flow capacity, indicates the absence of spillback. The fast switching between these two values implies the presence of transient spillback.

The computation presented above employs the LWR model with a Greenshields fundamental diagram (Greenshields, 1935). However, it is not difficult to conclude that such non-convergence will hold for any type of fundamental diagram. Such example reveals a technical difficulty arising from the theoretical investigation of the continuum approximation, although one may argue that modeling these phenomena exactly loses importance in large scale applications. Therefore, this should not completely diminish the value of the continuum signal model in the venue of engineering applications.

7. Numerical Study

The goal of this section is to numerically verify the convergence results and error analysis established in the previous sections. Let us again focus on the merge node depicted in Figure 1, with signal controls at the exits of I_1 , I_2 and I_3 . Two types of fundamental diagrams are considered in this numerical study: the triangular fundamental diagram (5.30) and the Greenshields fundamental diagram (Greenshields, 1935)

$$f(\rho) = \rho v_0 \left(1 - \frac{\rho}{\rho_j}\right) \quad (7.47)$$

where v_0 denotes the free-flow speed, ρ_j denotes the jam density. Link parameters related to these two fundamental diagrams are given in Table 1. For simplicity, all three links are assumed to have the same parameters.

	Free-flow speed (meter/second)	Jam density (vehicle/meter)	Critical density (vehicle/meter)	Flow capacity (vehicle/second)
Triangular fd	40/3	0.4	0.1	4/3
Greenshields fd	40/3	0.4	0.2	4/3

Table 1: Link parameters

7.1. Without spillback

Assume that the entrance of I_3 remains in the uncongested phase so that spillback does not occur. In addition, we let the signal control $u_1(t)$ for I_1 satisfy: $\Delta_A = 60$ seconds, $\eta_1 = 0.5$. Thus the theoretical error bound given by Theorem 4.4 is $\eta_1(1 - \eta_1)\Delta_A C_3 = 20$ (vehicles). The Moskowitz functions for I_1 are shown in Figure 9, where both the on-and-off signal model and the continuum signal model are employed. It is clearly observed that the continuum signalized junction model yields very good approximation to the one with the on-and-off signal controls, for both triangular and Greenshields fundamental diagrams. In particular, the absolute differences in the Moskowitz functions are uniformly bounded by 20 (vehicles) and are independent of time, which coincides with the theoretical result established in Theorem 4.4. We are also assured that such errors are almost unobservable using the normal scales of the Moskowitz functions.

7.2. With spillback

7.2.1. Triangular fundamental diagram

Assume that link I_3 is dominated by the congested phase, then the supply function $S_3(t)$ is illustrated in Figure 3. Let us now examine the difference $|N_{down}^{\Delta_A}(t) - N_{down}^0(t)|$ for link I_1 . First notice that it is entirely possible that whenever the control $u_1(t) = 1$, the supply $S_3(t) = 0$. In this case we have $N_{down}^{\Delta_A}(t) \equiv 0$ since no car can go through, while $N_{down}^0(t)$ is proportional to the integral of $S_3(t)$. Thus huge error is expected in this case. This is illustrated in Figure 10 with two different values of η_1 . We see from these figures that when spillback occurs, the errors grow with time roughly linearly and are within the theoretical bounds provided by (5.39). We also observe from the upper right picture that the established error bounds are tight, as they can be approached in some actual cases.

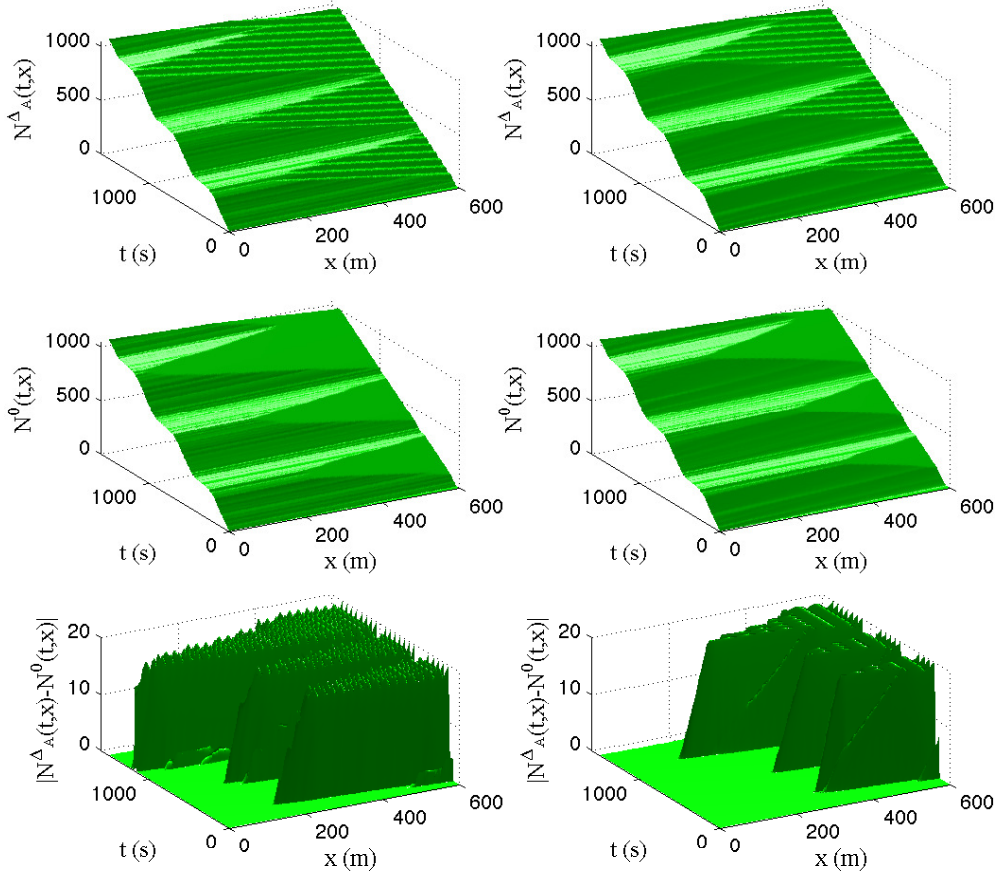


Figure 9: Moskowitz functions on link I_1 with the triangular fundamental diagram (left column) and the Greenshields fundamental diagram (right column). The first row corresponds to the on-and-off signal model; the second row corresponds to the continuum signal model; the third row presents the absolute differences in the Moskowitz functions from the first two rows.

7.2.2. Smooth and strictly concave fundamental diagram

Let us turn to the case with a strictly concave fundamental diagram, for instance, the Greenshields fundamental diagram. The damping effect on the flow variations caused by the strictly concave Greenshields fundamental diagram is demonstrated in Figure 11, where the supply at the entrance of I_3 is plotted with different choices of parameters. Notice that when the fundamental diagram $f(\cdot)$ takes the explicit form of (7.47), the upper bound on the jumps given by (5.42) is expressed more accurately as follows (Han et al., 2013c):

$$\frac{\rho_j v_0^2 \Delta_B}{4} \frac{2L + v_0 \Delta_B}{(L + v_0 \Delta_B)^2} \quad (7.48)$$

It is clearly observed from Figure 11 that while the exit flow of I_3 can have a big variation due to the presence of the signal $u_3(t)$, the supply function on the other end of the link has a reduced variation, in particular when the cycle Δ_B decreases and when the length L increases. This is

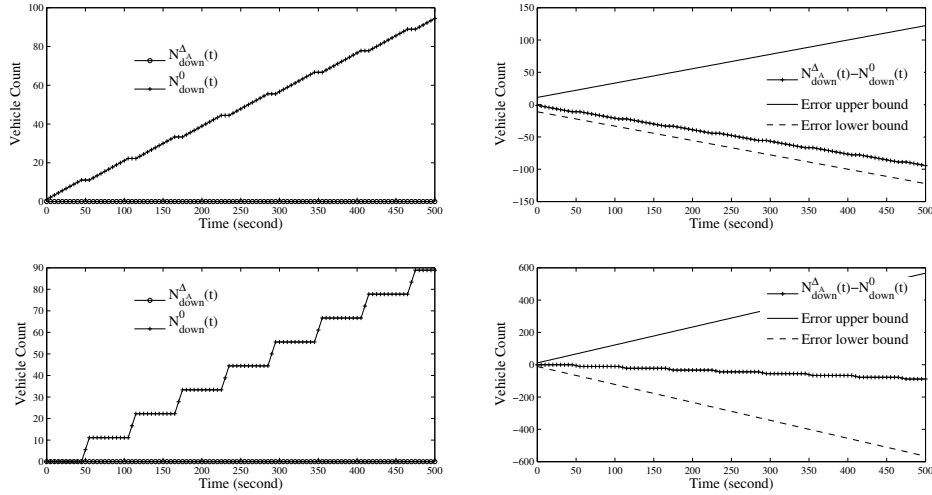


Figure 10: Comparison of $N_{down}^{AA}(t)$ and $N_{down}^0(t)$ under a specific scenario where $u_1(t) = 1 \implies S_3(t) = 0$. In this case $N_{down}^{AA}(t) \equiv 0$. First row: $\eta_1 = 1/6$. Second row: $\eta_1 = 5/6$.

consistent with (7.48). To further verify the bounds, Table 2 below compares the computed jumps in supply with the theoretical bound (7.48). From this table we see that the approximation error conveyed by inequality (5.40) (a) is valid and correct; and (b) provides a tight bound of the error.

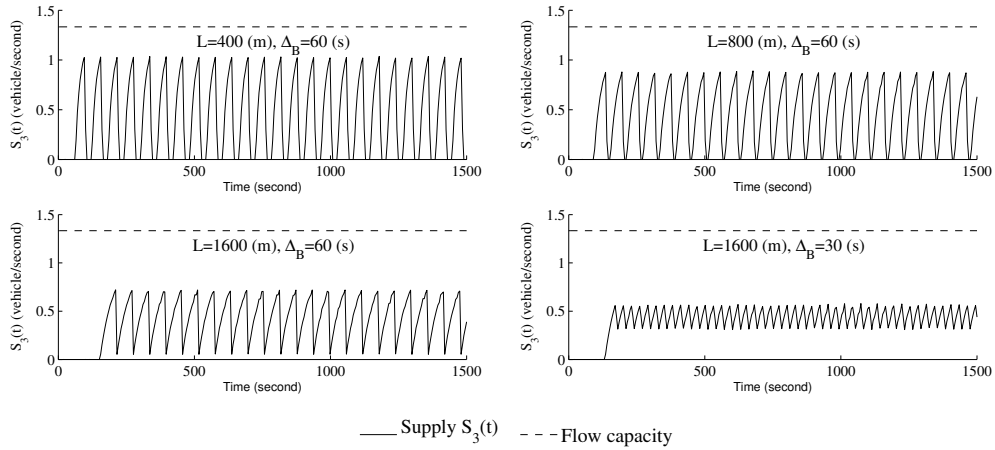


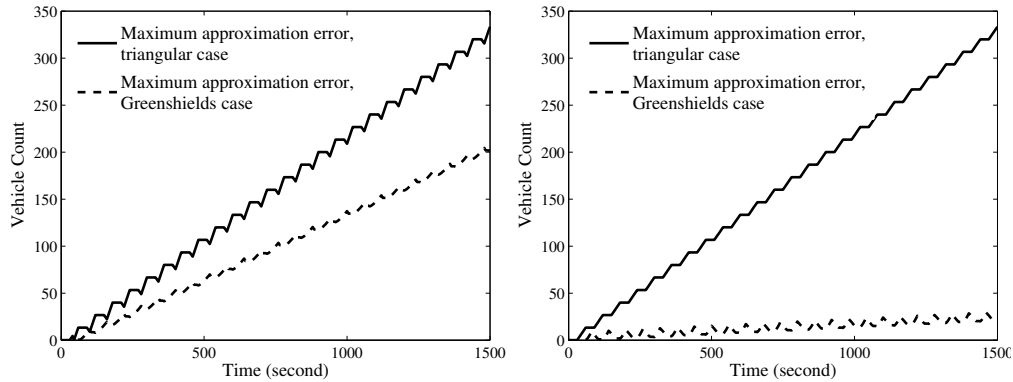
Figure 11: The supply function $S_3(t)$ at the entrance of link I_3 , when I_3 is dominated by the congested phase. The signal split for I_3 is fixed to be $1/3$. The broken lines indicate the link flow capacity. Several values of link length L and signal cycle Δ_B are considered, and the jumps in the supply are consistent with the theoretical bound (5.42).

In Theorem 5.4 we showed that the continuum approximation error grows with time when spillback occurs, and that the error increases roughly linearly for both the triangular fundamen-

	$L = 400$ (m) $\Delta_B = 60$ (s)	$L = 800$ (m) $\Delta_B = 60$ (s)	$L = 1600$ (m) $\Delta_B = 60$ (s)	$L = 1600$ (m) $\Delta_B = 30$ (s)
Computed jump	1.04	0.89	0.67	0.43
Theoretical bound	1.19	1.0	0.74	0.48

Table 2: Comparison of the actual jumps in the supply profile $S_3(t)$ with the theoretical bound on the jumps, when link I_3 is completely in the congested phase.

tal diagram and the strictly concave fundamental diagram, see (5.39) and (5.40). In order to numerical verify such results, we consider the merge junction from Figure 1 with link I_3 in the congested phase so that spillback occurs at intersection A . The traffic signal at intersection B has a cycle of 60 seconds and a split ration of $1/2$ for I_3 . The length of link I_3 is 400 meters. We set the signal cycle at A to be 60 seconds, and experiment with two different split values for I_1 : $\eta_1 = 1/3$ and $\eta_1 = 2/3$. Two cases with respectively the triangular fundamental diagram and with the Greenshields fundamental diagram, whose numerical specifications are provided in Table 1, are computed and the results are shown in Figure 12. The results indeed confirms that when spillback happens, both cases have errors that grow linearly with time. Moreover, the Greenshields case yields a smaller error, which coincides with out theoretical findings.

Figure 12: Linear growth of the maximum approximation error (MAE): $\max_{t,x} |N^{\Delta_A}(t, x) - N^0(t, x)|$, when spillback occurs at the intersection. The triangular case and the Greenshields case are compared. Left: $\eta_1 = 1/3$. Right: $\eta_1 = 2/3$. The case with the Greenshields fundamental diagram has a smaller error.

Finally, in Figure 13 we show the maximum absolute difference between $N^{\Delta}(t, x)$ and $N^0(t, x)$ of link I_1 for all $(t, x) \in [0, T] \times [a_1, b_1]$, when the downstream link I_3 is entirely congested. We show such error with both triangular and Greenshields fundamental diagrams and for different values of signal cycle Δ_A and split η_1 . Compared to the triangular fundamental diagram, the strictly concave (Greenshields) one yields a much lower error since the supply function $S_3(t)$ has a smaller variation due to the nonlinear effect discussed in Remark 5.2 and verified in Figure 11.

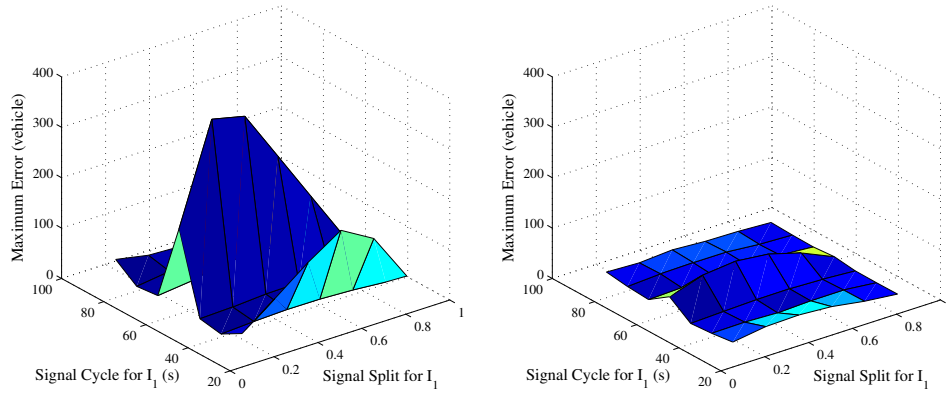


Figure 13: Maximum difference $|N^{\Delta_A}(t, x) - N^0(t, x)|$, $t \in [0, 1500]$ (second) for link I_1 , when the signal control for I_3 satisfies $\Delta_B = 60$ (second), $\eta_3 = 0.67$ and when I_3 is entirely in the congested phase (spillback occurs). Left: the triangular fundamental diagram. Right: the Greenshields fundamental diagram.

8. Application

8.1. Mixed integer linear programming approach for optimal signal control

In a signal optimization process usually realized by mixed integer mathematical programs, usage of the continuum signal model has several distinct advantages over the on-and-off one, such as those mentioned at the introductory part of this paper. This section presents a concrete example that demonstrates such advantages. We will provide two mixed integer linear programming (MILP) formulations using the continuum and the on-and-off signal models respectively, that aim at optimizing the dynamic network profile with proper constraints. Unlike many existing approaches that employ a cell-based dynamic, we consider a link-based kinematic wave model (Han et al., 2012b), also known as the *link transmission model* (Yperman et al., 2005), in order to reduce the number of (integer) variables involved in the program. These MILP formulations will not be elaborated here but are instead moved to the Appendix. A somewhat more comprehensive discussion of the MILP formulation is available in Han et al. (2012a).

8.2. Numerical experiment

In this section, we will solve the two mixed integer linear programs (MILP) using the on-and-off signal model and the continuum signal model respectively on the same traffic network. Performances of these two MILPs and their outcomes will be compared, which illustrates the advantages of using the continuum signal model over the on-and-off one.

We consider the network depicted in Figure 14 with three signalized intersections A , B and D . Note that node C is a diverge junction with no conflict of flows, therefore a signal control is not present. Traffic dynamics on each link are governed by the LWR model with a triangular fundamental diagram³. All the links in the network are assumed to have the same attributes as

³The demonstrated disadvantage of using the triangular fundamental diagram in the continuum signal model is circumvented by explicitly imposing in the programs that spillback does not occur at any junction. The reason is that: 1) a non-spillback situation is reasonable to maintain in a signal optimization process; and 2) the continuum model yields a good approximation of the on-and-off model in the absence of spillback.

given in Table 1. In addition, the length of each link is set to be 400 meters.

The signal cycle length and the time step in the on-and-off model is fixed to be 60 seconds and 10 seconds, respectively. In other words, signal control within each cycle is determined by six binary variables. For practical reasons, we stipulate that the green time and the red time must be no less than 20 seconds, so that the signal split variable can take on only three values: $1/3$, $1/2$, and $2/3$. Moreover, in order to adapt the signal controls to a dynamic decision environment, we allow the signal splits in both the on-and-off case and the continuum case to change every 5 minutes.

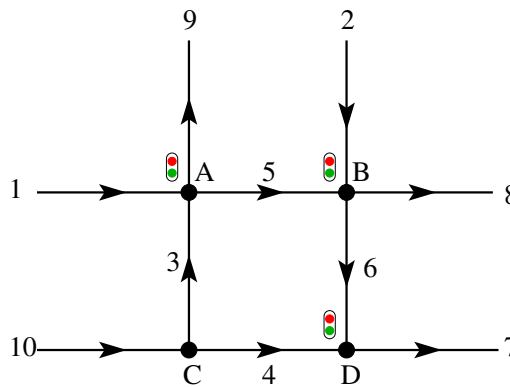


Figure 14: The test network where two MILPs are performed.

8.2.1. Performances of the two MILPs

The inflows into the test network are randomly generated and remain the same for all the computation scenarios mentioned below. Given that decisions on signal splits are made for every 5 minutes, we solve the MILPs on the network for time periods of 5, 10, 15, and 20 minutes. The computational times are presented in the first and second rows of Table 3⁴. Furthermore, we increase the time step size in the continuum case from 10 seconds to 30 seconds; this can be done since the time step in the continuum model is not constrained by the signal cycle or the split, which is in contrast to the on-and-off case. Results in such scenario is presented in the third row of Table 3. Notice that with a larger time step $h = 30$ seconds, the continuum-based MILP is capable of solving for a much larger time period, namely, one hour. This is shown in the last column of Table 3. In Table 4, we summarize some basic information of the MILPs such as the number of continuous or binary variables involved. The results again demonstrate the computational efficiency obtained by considering the continuum signal control.

8.2.2. Solution quality

In Table 5 we show, for a time period of 15 minutes, the optimal signal splits in the on-and-off case and in the continuum case provided by the two MILPs. We observe not only very different signal strategies in both cases, but also splits in the continuum case that are nontrivial and difficult to accommodate by the on-and-off signal model.

⁴All the MILPs were solved with CPLEX on the Penn State High Performance Computing Systems; see <http://rcc.its.psu.edu/resources/hpc/> for more details.

Time span	5 min	10 min	15 min	20 min	60 min
On and off ($h = 10$ s)	0.44 s	57.23 s	249.14 s	-	-
Continuum ($h = 10$ s)	0.25 s	9.50 s	49.42 s	241.32 s	-
Continuum ($h = 30$ s)	0.75 s	1.91 s	3.17 s	9.66 s	130.93 s

Table 3: Comparison of computational times of the MILPs. h denotes the time step size. “-” means that the MILP was not solved within the prescribed limit on computational time or memory usage.

# of CVs (# of BVs)	5 min	15 min	60 min
On and off ($h = 10$ s)	900 (600)	2700 (1800)	10800 (7200)
Continuum ($h = 30$ s)	400 (200)	1200 (600)	4800 (2400)

Table 4: Comparison of the number of continuous variables (CV) and the number of binary variables (BV) in the MILPs. h denotes the time step size.

	0 - 5 min		5 - 10 min		10 - 15 min	
	OA0	Cont	OA0	Cont	OA0	Cont
link 1	2/3	0.5	2/3	0.5	1/2	0.6957
link 2	2/3	0.6667	2/3	0.6667	2/3	0.7
link 3	1/3	0.5	1/3	0.5	1/2	0.3043
link 4	1/2	0.6333	1/3	0.6333	1/3	0.3
link 5	1/3	0.3333	1/3	0.3333	1/3	0.3
link 6	1/2	0.3667	2/3	0.3667	2/3	0.7

Table 5: Signal split for each link as a result of the MILPs with the on-and-off (OA0) signal control and the continuum (Cont) signal control.

In order to verify the approximation accuracy of the continuum signal model, we conduct the following calculation. The signal splits shown in Table 5 corresponding to the on-and-off case are taken as given parameters to simulate the dynamic signalized network using both on-and-off and continuum models. The respective network throughputs, expressed by the cumulative exiting vehicle counts on links 7, 8, and 9, are compared in Figure 15. Notice that for the continuum model, we employ both a smaller time step (10 seconds) and a larger time step (30 seconds) for comparison with the on-and-off case. The differences between these network throughputs are consistent with the established theoretical bounds, indicating the effectiveness of the continuum model in approximating the on-and-off model in the absence of vehicle spillback. In particular, we see that the continuum model yields a good approximation of the on-and-off model even when the time step increases significantly (30 seconds). This is because the error estimates established in Theorem 4.4 is in continuous time and independent of the time step selected for discrete-time computations. Such fact further illustrates the robustness of the continuum signal model.

9. Concluding remarks

This paper is concerned with a continuum signalized junction model as an approximation of the on-and-off signal model. We provide comprehensive theoretical and numerical results on the asymptotic behavior of the on-and-off signal model and its convergence to the corresponding continuum counterpart as the signal cycle tends to zero. We also provide estimations of

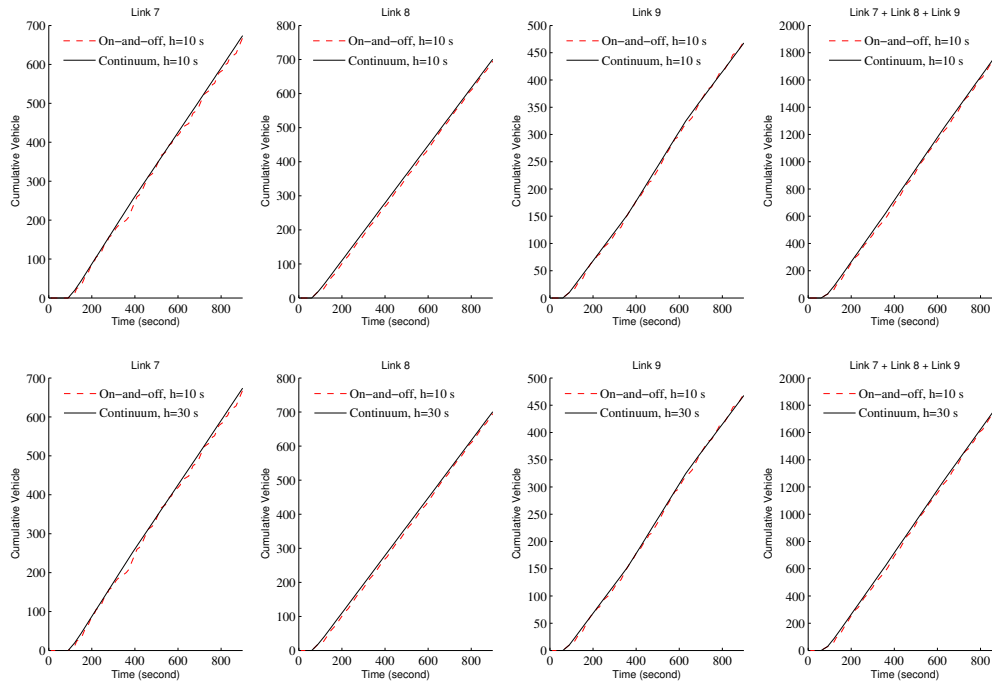


Figure 15: Comparisons of the cumulative exiting vehicle counts, which are obtained by using the on-and-off signal model and the continuum signal model with the same split parameters. First row: the on-and-off case vs. the continuum case with a time step of 10 seconds. Second row: the on-and-off case vs. the continuum case with a time step of 30 seconds.

the difference between the two types of signal models with non-infinitesimal cycles under various scenarios. The main findings and their implications can be summarized as follows. 1) The continuum signal model with any type of fundamental diagram yields a good approximation of the on-and-off model in the absence of spillback on the signalized network. 2) When spillback occurs somewhere in the network, the continuum approximation may or may not be accurate, depending on the fundamental diagram: if a triangular fundamental diagram is used, then the continuum model does not yield a good approximation; if the fundamental diagram is strictly concave, the continuum model approximates the on-and-off model relatively well and induces much smaller error. Note that even small errors can still be significant in some cases; e.g., when blocks are very short, a maximum error of 20 vehicles could be enough to fill an entire block. Thus, it is up to the analyst to determine if the continuum approximation is appropriate for a particular scenario. The error bounds provided here can be used to make this determination. As shown, these bounds depend on the cycle length and the capacity of the links impacted. In general, intersections with lower capacity links or smaller cycle lengths would be more appropriate for the continuum approximation model.

When spillback happens, the approximation error grows with time no matter what type of fundamental diagram is employed, and that error is closely related to ‘how concave’ the fundamental diagram is. Our technical interpretation of concavity in the fundamental diagram can be streamlined as follows in prose: the more concave a fundamental diagram is, the more nonlinear

its characteristic field is, and the more cancellation to the flow variation it causes, hence the less error we find in the approximation.

It should be noted that our results regarding the approximation efficacy of the continuum model in the presence of spillback are given in a quantitative way; that being said, we make no direct implication of which fundamental diagram is ‘good’ or ‘bad’ in the implementation of the continuum signal model. Rather, a specific fundamental diagram should be evaluated with, in addition to the error bounds provided in Section 4 and 5, other modeling or computational considerations and specific application scenarios.

Based on our technical results, we make the following inferences without formal proofs.

- In deriving the convergence results and the error estimates in the presence of spillback, the assumption of strict concavity needs only apply to the congested branch of the fundamental diagram. In other words, one can choose the uncongested branch arbitrarily as long as the minimum requirements (**F**) are satisfied, and the established results still hold. For example, one may consider a piecewise-defined fundamental diagram with a linear uncongested branch and a strictly concave congested branch.
- If a fundamental diagram has a piecewise linear congested branch, then the more the linear pieces, the less error the continuum approximation induces when spillback occurs. This can be explained rather intuitively by the wave-front tracking algorithm (Dafermos, 1972; Garavello and Piccoli, 2006). Nevertheless, the convergence result may not hold for the piecewise linear fundamental diagram in the presence of spillback.
- The continuum signal model and our methodological framework are easily generalizable to a signal junction with m incoming links and n outgoing links, where $m > 1$, $n \geq 1$. One example – a junction with two incoming links and two outgoing links – is provided in Appendix A.3.

This paper is the first to rigorously analyze the continuum junction model that employs a traffic signal control mechanism, and to provide foundation and guidance for the applications of such model, which is an efficient and flexible alternative to the on-and-off signal model. Results developed in this paper have a positive impact on dynamic traffic assignment, especially on the network performance submodel, which describes flow propagation, flow conservation, and travel delay on signalized networks. In particular, when certain types of DTA problems are to be solved using the continuum signal model, our findings made in this paper provide practitioners with suggestions regarding the choice of fundamental diagrams, depending on whether or not spillback occurs, and with ways of assessing the approximation efficacy of the continuum model, based on the error estimates that we established. Immediate applications of the continuum signal model to DTA are under way. It also remains an important aspect of theoretical investigation to extend our methodological framework to other traffic flow dynamics, such as the link delay model (Friesz et al., 1993) and the Vickrey model (Vickrey, 1969; Han et al., 2013a,b), and to accommodate more complicated turning movements at junctions.

Appendix A. Two mixed integer linear programs for optimal signal control

Appendix A.1. The link-based kinematic wave model (LKWM)

Discussion of the LKWM below follows Han et al. (2012a), and the resulting discrete-time model is equivalent to the link transmission model proposed by Yperman et al. (2005).

Let us consider a homogeneous link $[a, b]$, whose dynamic is governed by the LWR model. A triangular fundamental diagram is used with the same set of notations as given in (5.30). Define a binary variable $\bar{r}(t)$ that indicates whether the entrance of the link is in the free-flow phase ($\bar{r}(t) = 0$) or in the congested phase ($\bar{r}(t) = 1$). A similar notation $\hat{r}(t)$ is used for the exit of the link. We also define the entering flow $\bar{q}(t)$ and the exiting flow $\hat{q}(t)$ of the link. The variational theory then asserts that

$$\bar{r}(t) = \begin{cases} 1, & \text{if } \int_0^t \bar{q}(\tau) d\tau = \int_0^{t-\frac{L}{w}} \hat{q}(\tau) d\tau + \rho_j L \\ 0, & \text{if } \int_0^t \bar{q}(\tau) d\tau < \int_0^{t-\frac{L}{w}} \hat{q}(\tau) d\tau + \rho_j L \end{cases} \quad (\text{A.1})$$

$$\hat{r}(t) = \begin{cases} 0, & \text{if } \int_0^{t-\frac{L}{v}} \bar{q}(\tau) d\tau = \int_0^t \hat{q}(\tau) d\tau \\ 1, & \text{if } \int_0^{t-\frac{L}{v}} \bar{q}(\tau) d\tau > \int_0^t \hat{q}(\tau) d\tau \end{cases} \quad (\text{A.2})$$

where v and w denote the forward and backward wave speeds respectively, ρ_j denotes the jam density and L denotes the link length.

Appendix A.2. Discrete-time formulation of the traffic dynamics

We discretize Eqn. (A.1) and (A.2) to get the mixed integer program. Let us begin with some discrete-time notations for each link I_i , where the superscript k always indicates the time step.

\bar{q}_i^k	the flow at which vehicles enter link I_i ,
\hat{q}_i^k	the flow at which vehicles exit link I_i ,
\bar{r}_i^k	the binary variable that indicates the traffic phase at the entrance of I_i ,
\hat{r}_i^k	the binary variable that indicates the traffic phase at the exit of I_i ,
S_i^k	the supply of link I_i ,
D_i^k	the demand of link I_i ,
u_i^k	the binary signal control variable for link I_i ,
η_i^k	the continuum priority parameter for link I_i ,

Fix a time step size h , we define $\Delta_i^f \doteq \frac{L_i}{v_i h}$, $\Delta_i^b \doteq \frac{L_i}{w_i h}$. Note that both Δ_i^f and Δ_i^b are rounded up to the nearest integer if they are not already integers. We are now ready to state the discrete versions of (A.1)-(A.2) as follows.

$$\begin{cases} h \sum_{k=1}^{l-\Delta_i^b} \hat{q}_i^k - h \sum_{k=1}^l \bar{q}_i^k + \rho_{j,i} L_i = \mathcal{M}(1 - \bar{r}_i^l) \\ h \sum_{k=1}^{l-\Delta_i^b} \hat{q}_i^k - h \sum_{k=1}^l \bar{q}_i^k + \rho_{j,i} L_i > -\mathcal{M}\bar{r}_i^l \end{cases} \quad \forall i, \forall l \quad (\text{A.3})$$

$$\begin{cases} h \sum_{k=1}^{l-\Delta_i^f} \bar{q}_i^k - h \sum_{k=1}^l \hat{q}_i^k = \mathcal{M}\hat{r}_i^l \\ h \sum_{k=1}^{l-\Delta_i^f} \bar{q}_i^k - h \sum_{k=1}^l \hat{q}_i^k > \mathcal{M}(\hat{r}_i^l - 1) \end{cases} \quad \forall i, \forall l \quad (\text{A.4})$$

where $\mathcal{M} > 0$ is a large constant, $\rho_{j,i}$ and L_i denote respectively the jam density and length of link I_i . Throughout this section, we stipulate that the entrance of every link of the network remains in the uncongested phase so that spillback does not occur. There are two reasons for this: 1) the non-spillback situation is reasonable to maintain in a signal optimization process; 2) the continuum model yields a good approximation of the on-and-off model in the absence of spillback. With this in mind, we must have $\tilde{r}_i^k \equiv 0$ for all i and k , thus (A.4) reduces to

$$h \sum_{k=1}^{l-\Delta_i^f} \bar{q}_i^k - h \sum_{k=1}^l \hat{q}_i^k = 0 \quad \forall i, \forall l \quad (\text{A.5})$$

Moreover, the demand D_i^k , whose continuous-time expression is given by (2.2), is now determined via the following inequalities, where C_i denotes the flow capacity of link I_i

$$\begin{cases} C_i + \mathcal{M}(\tilde{r}_i^k - 1) \leq D_i^k \leq C_i \\ \bar{q}_i^{k-\Delta_i^f} - \mathcal{M}\tilde{r}_i^k \leq D_i^k \leq \bar{q}_i^{k-\Delta_i^f} + \mathcal{M}\tilde{r}_i^k \end{cases} \quad \forall i, \forall k \quad (\text{A.6})$$

Appendix A.3. Dynamics at signalized junctions

We relate our expression of the discrete network dynamics to two specific types of signalized junctions depicted in Figure A.16.

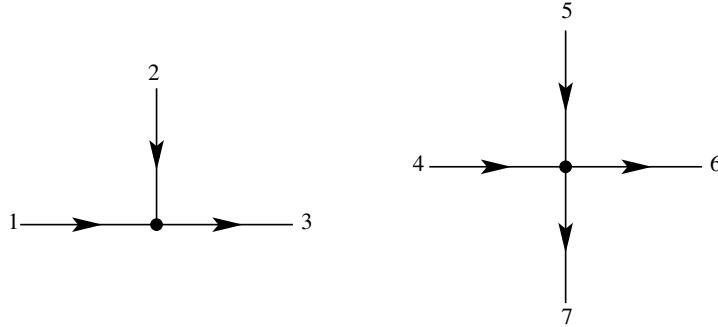


Figure A.16: Two signalized junctions

- Regarding the merge junction on the left of Figure A.16, the continuous-time dynamics are already given by (2.7) and (2.8) for the on-and-off model and the continuum model respectively. Therefore, the discrete-time formulations are:

$$\left. \begin{aligned} \hat{q}_1^k &= \min \{ D_1^k, \min \{ C_1, C_3 \} \cdot u_1^k \} \\ \hat{q}_2^k &= \min \{ D_2^k, \min \{ C_2, C_3 \} \cdot u_2^k \} \\ \bar{q}_3^k &= \hat{q}_1^k + \hat{q}_2^k \end{aligned} \right\} \quad \text{On-and-off model} \quad (\text{A.7})$$

$$\left. \begin{aligned} \hat{q}_1^k &= \min \{ D_1^k, \min \{ C_1, C_3 \} \cdot \eta_1^k \} \\ \hat{q}_2^k &= \min \{ D_2^k, \min \{ C_2, C_3 \} \cdot \eta_2^k \} \\ \bar{q}_3^k &= \hat{q}_1^k + \hat{q}_2^k \end{aligned} \right\} \quad \text{Continuum model} \quad (\text{A.8})$$

- For the intersection on the right of Figure A.16, we need to introduce additional turning rates $\alpha_{4,6} + \alpha_{4,7} = 1$, $\alpha_{5,6} + \alpha_{5,7} = 1$. It is straightforward to verify that the on-and-off and the continuum models are:

$$\left. \begin{aligned} \hat{q}_4^k &= \min \left\{ D_4^k, \min \left\{ C_4, \frac{C_6}{\alpha_{4,6}}, \frac{C_7}{\alpha_{4,7}} \right\} \cdot u_4^k \right\} \\ \hat{q}_5^k &= \min \left\{ D_5^k, \min \left\{ C_5, \frac{C_6}{\alpha_{5,6}}, \frac{C_7}{\alpha_{5,7}} \right\} \cdot u_5^k \right\} \\ \bar{q}_6^k &= \alpha_{4,6} \hat{q}_4^k + \alpha_{5,6} \hat{q}_5^k, \quad \bar{q}_7^k = \alpha_{4,7} \hat{q}_4^k + \alpha_{5,7} \hat{q}_5^k \end{aligned} \right\} \text{ On-and-off model} \quad (\text{A.9})$$

$$\left. \begin{aligned} \hat{q}_4^k &= \min \left\{ D_4^k, \min \left\{ C_4, \frac{C_6}{\alpha_{4,6}}, \frac{C_7}{\alpha_{4,7}} \right\} \cdot \eta_4^k \right\} \\ \hat{q}_5^k &= \min \left\{ D_5^k, \min \left\{ C_5, \frac{C_6}{\alpha_{5,6}}, \frac{C_7}{\alpha_{5,7}} \right\} \cdot \eta_5^k \right\} \\ \bar{q}_6^k &= \alpha_{4,6} \hat{q}_4^k + \alpha_{5,6} \hat{q}_5^k, \quad \bar{q}_7^k = \alpha_{4,7} \hat{q}_4^k + \alpha_{5,7} \hat{q}_5^k \end{aligned} \right\} \text{ Continuum model} \quad (\text{A.10})$$

It remains to express the operator $\min(\cdot)$ appearing in (A.7)-(A.10) as a set of linear inequalities by using additional binary variables, which, due to space limitation, will not be elaborated in this paper. The reader is referred to Han et al. (2012a) for more detail.

Finally, one has a lot of flexibility in choosing the objective function once the constraints are articulated as above. For our specific example presented in Section 8.2 and Figure 14, the following linear objective function is selected:

$$\text{maximize} \quad \sum_{k=1}^N \frac{1}{k+1} (\hat{q}_7^k + \hat{q}_8^k + \hat{q}_9^k) \quad (\text{A.11})$$

where N is the total number of time intervals. Choosing such objective function ensures that the throughput of the network is maximized at any instance of time.

To summarize, for the problem of finding optimal signal timing that avoids spillback, the mixed integer linear program with the on-and-off signal model is given by (A.3), (A.5), (A.6), (A.7), (A.9) and (A.11); the MILP with the continuum model is given by (A.3), (A.5), (A.6), (A.8), (A.10) and (A.11). Notice that both programs may be subject to some additional constraints, e.g., no conflict in signal lights, upper and lower bounds on green and red time, and so forth. These are quite straightforward and are omitted from this paper.

References

- Aubin, J.P., Bayen, A.M., Saint-Pierre, P., 2008. Dirichlet problems for some Hamilton-Jacobi equations with inequality constraints. *SIAM Journal on Control and Optimization* 47 (5), 2348-2380.
- Aziz, H.M., Ukkusuri, S.V., 2012. Unified framework for dynamic traffic assignment and signal control with cell transmission model. *Transportation Research Record*, 2311, 73-84.
- Barron, E.N., Jensen, R., 1990. Semicontinuous viscosity solutions for Hamilton-Jacobi equations with convex Hamiltonians. *Communications in Partial Differential Equations* 15 (12), 293-309.
- Bressan, A., 2000. *Hyperbolic Systems of Conservation Laws. The One Dimensional Cauchy Problem*. Oxford University Press.
- Bressan, A., Han, K., 2011. Optima and equilibria for a model of traffic flow. *SIAM Journal on Mathematical Analysis*, 43 (5), 2384-2417.
- Chitour, Y., Piccoli, B., 2005. Traffic circles and timing of traffic lights for cars flow. *Discrete and Continuous Dynamical Systems - Series B* 5 (3), 599-630.
- Claudel, C.G., Bayen, A.M., 2010. Lax-Hopf Based incorporation of internal boundary conditions into Hamilton-Jacobi equation. Part I: Theory. *IEEE Transactions on Automatic Control* 55 (5), 1142-1157.
- Claudel, C.G., Bayen, A.M., 2010. Lax-Hopf based incorporation of internal boundary conditions into Hamilton-Jacobi equation. Part II: Computational methods. *IEEE Transactions on Automatic Control* 55 (5), 1158-1174.

-
- Dafermos, C.M., 1972. Polygonal approximations of solutions of the initial value problem for a conservation law. *Journal of Mathematical Analysis and Applications* 38 (1), 33-41.
- Daganzo, C.F., 1994. The cell transmission model: A simple dynamic representation of highway traffic. *Transportation Research Part B* 28 (4), 269-287.
- Daganzo, C.F., 1995. The cell transmission model, part II: network traffic. *Transportation Research Part B* 29 (2), 79-93.
- Daganzo, C.F., 2005. A variational formulation of kinematic waves: basic theory and complex boundary conditions. *Transportation Research Part B* 39 (2), 187-196.
- Frankowska, H., 1993. Lower semicontinuous solutions of Hamilton-Jacobi-Bellman equations. *SIAM Journal on Control and Optimization* 31 (1), 257-272.
- Friesz, T.L., Bernstein, D., Smith, T., Tobin, R., Wie, B., 1993. A variational inequality formulation of the dynamic network user equilibrium problem. *Operations Research* 41 (1), 80-91.
- Friesz, T.L., Han, K., Neto, P.A., Meimand, A., Yao, T., 2012. Dynamic user equilibrium based on a hydrodynamic model. *Transportation Research Part B* 47 (1), 102-126.
- Garavello, M., Piccoli, B., 2006. *Traffic Flow on Networks. Conservation Laws Models*. AIMS Series on Applied Mathematics, Springfield, Mo..
- Gayah, V.V., Daganzo, C.F., 2012. Analytical capacity comparison of one-way and two-way signalized street networks. *Transportation Research Record* 2301, 76-85.
- Ge, Y.E., Zhou, X., 2012. An alternative definition of dynamic user optimum on signalised road networks. *Journal of Advanced Transportation* 46 (3), 236-253.
- Guler, S.I., Cassidy, M.J., 2012. Strategies for sharing bottleneck capacity among buses and cars. *Transportation Research Part B* 46 (10), 1334-1345.
- Greenshields, B.D., 1935. A study of traffic capacity. In *Proceedings of the 13th Annual Meeting of the Highway Research Board* 14, 448-477.
- Han, K., 2013. An analytical approach to sustainable transportation network design. Ph.D. dissertation, Pennsylvania State University.
- Han, K., Friesz, T.L., Yao, T., 2012a. A link-based mixed integer LP approach for adaptive traffic signal control. Preprint available online at <http://arxiv.org/abs/1211.4625>
- Han, K., Friesz, T.L., Yao, T., 2013a. A partial differential equation formulation of Vickrey's bottleneck model, part I: Methodology and theoretical analysis. *Transportation Research Part B* 49, 55-74.
- Han, K., Friesz, T.L., Yao, T., 2013b. A partial differential equation formulation of Vickrey's bottleneck model, part II: Numerical analysis and computation. *Transportation Research Part B* 49, 75-93.
- Han, K., Piccoli, B., Friesz, T.L., Yao, T., 2012b. A continuous-time link-based kinematic wave model for dynamic traffic networks. Preprint available online at <http://arxiv.org/abs/1208.5141>
- Han, K., Piccoli, B., Friesz, T.L., Yao, T., 2013c. On the continuum approximation of the on-and-off signal control on dynamic traffic networks. *Transportation Research Board 93rd Annual Meeting*, Washing D.C..
- Improta, G., Cantarella, G.E., 1984. Control system design for an individual signalized junction. *Transportation Research Part B* 18 (2), 147-167.
- Lebacque, J., Khoshyaran, M., 1999. Modeling vehicular traffic flow on networks using macroscopic models, in *Finite Volumes for Complex Applications II*, 551-558, Hermes Sci. Publ., Paris, 1999.
- Lighthill, M., Whitham, G., 1955. On kinematic waves. II. A theory of traffic flow on long crowded roads. *Proceedings of the Royal Society of London: Series A* 229, 317-345.
- Lin, W.H., Wang, C., 2004. An enhanced 0 - 1 mixed-integer LP formulation for traffic signal control. *IEEE Transactions on Intelligent transportation systems* 5 (4), 238-245.
- Lo, H., 1999a. A novel traffic signal control formulation. *Transportation Research Part A* 33 (6), 433-448.
- Lo, H., 1999b. A cell-based traffic control formulation: strategies and benefits of dynamic timing plans. *Transportation Science* 35 (2), 148-164.
- Miller, A.J., 1963. Computer control system for traffic networks. *Proceedings of the 2nd International Symposium on Theory of Traffic Flow*, London, UK.
- Moskowitz, K., 1965. Discussion of 'freeway level of service as influenced by volume and capacity characteristics' by D.R. Drew and C.J. Keese. *Highway Research Record*, 99, 43-44.
- Newell, G. F. (1993). A simplified theory of kinematic waves in highway traffic. Part I: General theory. *Transportation Research Part B* 27 (4), 281-287.
- Richards, P.I., 1956. Shockwaves on the highway. *Operations Research* 4 (1), 42-51.
- Robertson, D.J., Bretherton, R.D., 1974. Optimal control of an intersection for any known sequences of vehicle arrivals. *Proceedings of the 2nd IFAC-IFIP-IFORS Symposium on Traffic Control and Transport Systems*, Monte Carlo.
- Shelby, S., 2004. Single-intersection evaluation of real-time adaptive traffic signal control algorithms. *Transportation Research Record* 1867, 183-192.
- Smith M.J., 2010. Intelligent network control: using an assignment-control model to design fixed time signal timings. In *New Developments in Transport Planning: Advances in Dynamic Traffic Assignment*, Tempere CMJ, Viti F, Immers

ARTICLE LINK: <http://www.sciencedirect.com/science/article/pii/S0191261514000022>

PLEASE CITE THIS ARTICLE AS

Han, K., Gayah, V.V., Piccoli, B., Friesz, T.L., Yao, T., 2015. On the continuum approximation of the on-and-off signal control on dynamic traffic networks.

Transportation Research Part B 61, 73-97.

LH (eds). Edward Elgar: Cheltenham, UK, 57-71.

Szeto, W.Y., Lo, H.K., 2006. Dynamic traffic assignment: Properties and extensions. *Transportmetrica* 2 (1), 31-52.

Vickrey, W.S., 1969. Congestion theory and transport investment. *The American Economic Review* 59 (2), 251-261.

Ukkusuri, S., Doan, K., Azzi, H.M., 2013. A bi-level formulation for the combined dynamic equilibrium based traffic signal control. *Procedia - Social and Behavioral Sciences* 80, 729-752.

Yperman, I., Logghe, S., Immers, L., 2005. The Link Transmission Model: An Efficient Implementation of the Kinematic Wave Theory in Traffic Networks, *Advanced OR and AI Methods in Transportation, Proc. 10th EWGT Meeting and 16th Mini-EURO Conference, Poznan, Poland, 122-127*, Publishing House of Poznan University of Technology.